MTP-AERO-63-34 OTS
May 14, 1963

N63 22196

CODE-1

50p.

GEORGE C. MARSHALL SPACE FLIGHT CENTER

HUNTSVILLE, ALABAMA

(NASA TMX 50869)

WIND TUNNEL AND LABORATORY TESTS ON THE EDCLIFF 4-15 ANGLE OF PITCH AND YAW TRANSDUCER SUMMARY REPORT

By

Aeroballistics Division

5 refs

OTS PRICE

XEROX $ 4.60 ph

MICROFILM $ 1.70 mf

NASA

[redacted]

NATIONAL AERONAUTICS AND SPACE ADMINISTRATION

MSFC - Form 523 (Rev. November 1960)

GEORGE C. MARSHALL SPACE FLIGHT CENTER

MTP-AERO-63-34

WIND TUNNEL AND LABORATORY TESTS ON THE EDCLIFF 4-15 ANGLE OF PITCH AND YAW TRANSDUCER SUMMARY REPORT

By

Aeroballistics Division

ABSTRACT

22196

This report summarizes the results of laboratory and wind tunnel tests performed on the Edcliff 4-15 angle of pitch and yaw transducer, P/N 108760-E, S/N 118 and 119. Correlations between transducer measurements made in the laboratory and the characteristics of the transducer in flight as determined from the test programs are presented. Laboratory measurements included calibration of the readout potentiometers, measurement of the viscous damping factor, measurement of the mass unbalance, and measurement of the torque required to overcome static friction.

The wind tunnels used were the Langley Research Center 8 x 8-Foot Transonic Pressure Tunnel, and the 20-Inch Supersonic Wind Tunnel at the Jet Propulsion Laboratory. The Mach number range of the tests was 0.2 to 4.54. The static and dynamic characteristics of the transducer through this Mach number range were determined. Included in the report are graphs and a table of the indicated transducer output versus input angle of pitch. At Mach numbers greater than 1.40, the output-input relationship is linear within ±0.4 degree; in the transonic region it is linear within ±0.9 degree.

Static response wind tunnel data indicated an aerodynamic-mechanical misalignment of 0.05 degree for one sensor. Variation in mechanical-electrical alignment was determined from calibrations taken before and after testing with indicated differences as great as 0.18 degree. Test experience indicates that final aerodynamic-mechanical-electrical zero alignment can logically be expected to fall within ±0.2°.

The dynamic behavior was also analyzed at each Mach number, using the response of the transducer to a three-degree step change in angle

of pitch. These dynamic characteristics are presented in this report. The natural frequency characteristic of the transducer at the various Mach numbers varied from 32 to 157 radians per second.

The damping ratio determined in the wind tunnel varied from 0.2 to 1.4 critical. This was less than predicted, and in order to correlate the damping observed in the tunnels with laboratory damping measurements, it is necessary to assume that the damping decreased due to the heating effect of energy being dissipated in the internal viscous dampers. The dynamic response at low pressures was not consistent with the expected second order response.

GEORGE C. MARSHALL SPACE FLIGHT CENTER

MTP-AERO-63-34

May 14, 1963

WIND TUNNEL AND LABORATORY TESTS ON THE EDCLIFF 4-15 ANGLE OF PITCH AND YAW TRANSDUCER SUMMARY REPORT

By

Aeroballistics Division

EXPERIMENTAL AERODYNAMICS BRANCH
AEROBALLISTICS DIVISION

TABLE OF CONTENTS

Page

SECTION I. INTRODUCTION

Introduction 1

SECTION II. WIND TUNNEL CONDITIONS

Wind Tunnel Conditions 8

SECTION III. STATIC RESPONSE CHARACTERISTICS

A. Preliminary Laboratory Measurements. 11
B. Zero Shift 12
C. Static Angle of Attack Response. 17

SECTION IV. DYNAMIC RESPONSE CHARACTERISTICS

A. Calculations 22
B. Preliminary Laboratory Measurements. 27
C. Test Results 28

SECTION V. CONCLUDING REMARKS

Concluding Remarks 39

SECTION VI. REFERENCES

References 40

LIST OF ILLUSTRATIONS

Figure	Title	Page
1.	Outline of Edcliff 4-15 Angle of Pitch and Yaw Transducer Mounted on the Two Sting Assemblies	2
2.	Photographs of Edcliff 4-15 Transducer Mounted in LRC Tunnel on Two Sting Assemblies (MSFC Calibration Fixture Visible in Upper Photograph)	4
3.	Photographs of Edcliff 4-15 Transducer Mounted in JPL Tunnel on Two Sting Assemblies	5
4.	Schlieren Photographs of Edcliff 4-15 Transducer in LRC and JPL Wind Tunnels	6
5.	Characteristics of a Typical Trajectory of a Liquid Propelled Booster	9
6.	Wind Tunnel Conditions	10
7.	Zero Shift Caused by Geometrical Asymmetry on Pitch Axis of Transducer S/N 119	15
8.	Apparent Geometrical Asymmetry Using Both Straight and Step Sting Data	18
9.	Zero Corrected Static Response Data, LRC Tunnel	18
10.	Zero Corrected Static Response Data, JPL Tunnel	19
11.	Slope (About Zero) of Static Output Angle with Respect to Set Input Angle	20
12.	Zero Corrected Angle of Pitch Static Response Data for 6-Degree Angle of Yaw	21
13.	Torque Coefficient Derivation Computed from Previously Established Aerodynamics of the Transducer Geometry	24
14.	Aerodynamic Damping Factor	26
15.	Laboratory Measurements of Viscous Damping Factor of Transducer S/N 119	29
16.	Typical Dynamic Response Oscillograph Trace	30
17.	Undamped Natural Frequencies and Damping Ratios Reduced from Wind Tunnel Dynamic Tests	31
18.	Damping Factor Measured in Wind Tunnel	33

Figure	Title	Page
19.	Difference Between Predicted and Measured Damping Factors, and Corrections Proportional to Turbulent Heating Rate	34
20.	Ratio of Undamped Natural Frequency and the Square Root of Dynamic Pressure	37
21.	Dynamic Response Typical of All Data of Tests at Mach 0.2 and 4.54	38

DEFINITION OF SYMBOLS

Symbol	Definition
A	Base area of transducer = 81.0 centimeters^2
B	Damping factor = damping torque/$\dot{\theta}$, gram centimeter second/radian
C_{M_θ}	Torque coefficient derivative with respect to θ about zero, 1/radian
I	Longitudinal moment of inertia of transducer about center of rotation = 6.71 gram-centimeter-seconds^2
K	Aerodynamic spring constant, gram centimeters
M	Mach number
q	Dynamic pressure, kiloponds/meter^2
T	Torque, gram centimeters
V	Velocity, kilometers/second
ζ	Damping ratio (fraction of critical damping)
θ	Angle between transducer head and airflow direction, radians
ω_n	Undamped natural frequency, radians/second

GEORGE C. MARSHALL SPACE FLIGHT CENTER

MTP-AERO-63-34

WIND TUNNEL AND LABORATORY TESTS ON THE EDCLIFF 4-15 ANGLE OF PITCH AND YAW TRANSDUCER SUMMARY REPORT

By

Aeroballistics Division

SUMMARY

This report summarizes the results of laboratory and wind tunnel tests performed on the Edcliff 4-15 angle of pitch and yaw transducer, P/N 108760-E, S/N 118 and 119. Correlations between transducer measurements made in the laboratory and the characteristics of the transducer in flight as determined from the test programs are presented. Laboratory measurement of the viscous damping factor, measurement of the mass unbalance, and measurement of the torque required to overcome static friction.

The wind tunnels used were the Langley Research Center 8 x 8-Foot Transonic Pressure Tunnel, and the 20-Inch Supersonic Wind Tunnel at the Jet Propulsion Laboratory. The Mach number range of the tests was 0.2 to 4.54. The static and dynamic characteristics of the transducer through this Mach number range were determined. Included in the report are graphs and a table of the indicated transducer output versus input angle of pitch. At Mach numbers greater than 1.40, the output-input relationship is linear within ±0.4 degree; in the transonic region it is linear within ±0.9 degree.

Static response wind tunnel data indicated an aerodynamic-mechanical misalignment of 0.05 degree for one sensor. Variation in mechanical-electrical alignment was determined from calibrations taken before and after testing with indicated differences as great as 0.18 degree. Test experience indicates that final aerodynamic-mechanical-electrical zero alignment can logically be expected to fall within ±0.2 degree.

The dynamic behavior was also analyzed at each Mach number, using the response of the transducer to a three-degree step change in angle of pitch. These dynamic characteristics are presented in this report. The natural frequency characteristic of the transducer at the various Mach numbers varied from 32 to 157 radians per second.

The damping ratio determined in the wind tunnel varied from 0.2 to 1.4 critical. This was less than predicted and, in order to correlate the damping observed in the tunnels with laboratory damping measurements, it is necessary to assume that the damping decreased due to the heating effect of energy being dissipated in the internal viscous dampers. The dynamic response at low pressures was not consistent with the expected second-order response.

SECTION I. INTRODUCTION

This report is a summary of laboratory and wind tunnel tests performed on the Edcliff 4-15 Angle of Pitch and Yaw Transducer, P/N 108760-E. The angle of pitch and yaw transducer tested is a boom-mounted two-axis sensor that is aligned with the direction of the airflow by aerodynamic force. The movable outer surface of the transducer is a conical body of revolution with a spherical, blunted nose. The outline dimensions are shown in Figure 1. The tested version has an aluminum body, internal viscous (silicon fluid) dampers on both axes, and a range of ±15 degrees on both axes. The outputs are potentiometer positions. The mounting boom is a one-inch-diameter stainless steel tube.

Two P/N 108760-E transducers were used in the test program and are identified by Serial Numbers 118 and 119. Laboratory tests were conducted on these transducers at the Nortronics Research Park facility, Palos Verdes Estates, California, prior to the wind tunnel tests. The laboratory tests established mechanical-electrical calibration, damping factor, starting friction, and mass unbalance, which is defined as non-coincidence of the center of gravity and center of rotation of the movable head.

From 5 June to 8 June 1962, wind tunnel tests of the transducers were conducted in the Langley Research Center (LRC) 8 x 8-foot pressure tunnel, at Mach numbers of 0.2, 0.6, 0.8, 0.9, 1.0, and 1.2. (Reference 1 describes the LRC tunnel.) From 30 June to 5 July 1962, wind tunnel tests were conducted in the Jet Propulsion Laboratory (JPL) 20-inch supersonic wind tunnel, at Mach numbers of 1.40, 1.65, 2.01, 3.01, and 4.54 (Reference 1 describes the JPL tunnel). The wind tunnel test conditions are summarized in Section II.

Two sting assemblies were used in the wind tunnel installations. Figure 1 includes outlines of both assemblies; they are referred to as the step sting and the straight sting. Figure 2 shows photographs of the transducer mounted in the LRC wind tunnel with the two stings. Figure 3 shows two similar views in the JPL wind tunnel. Figure 4 shows two Schlieren photographs of the transducer operating in the LRC and JPL wind tunnels at the indicated angle of attack and Mach number conditions.

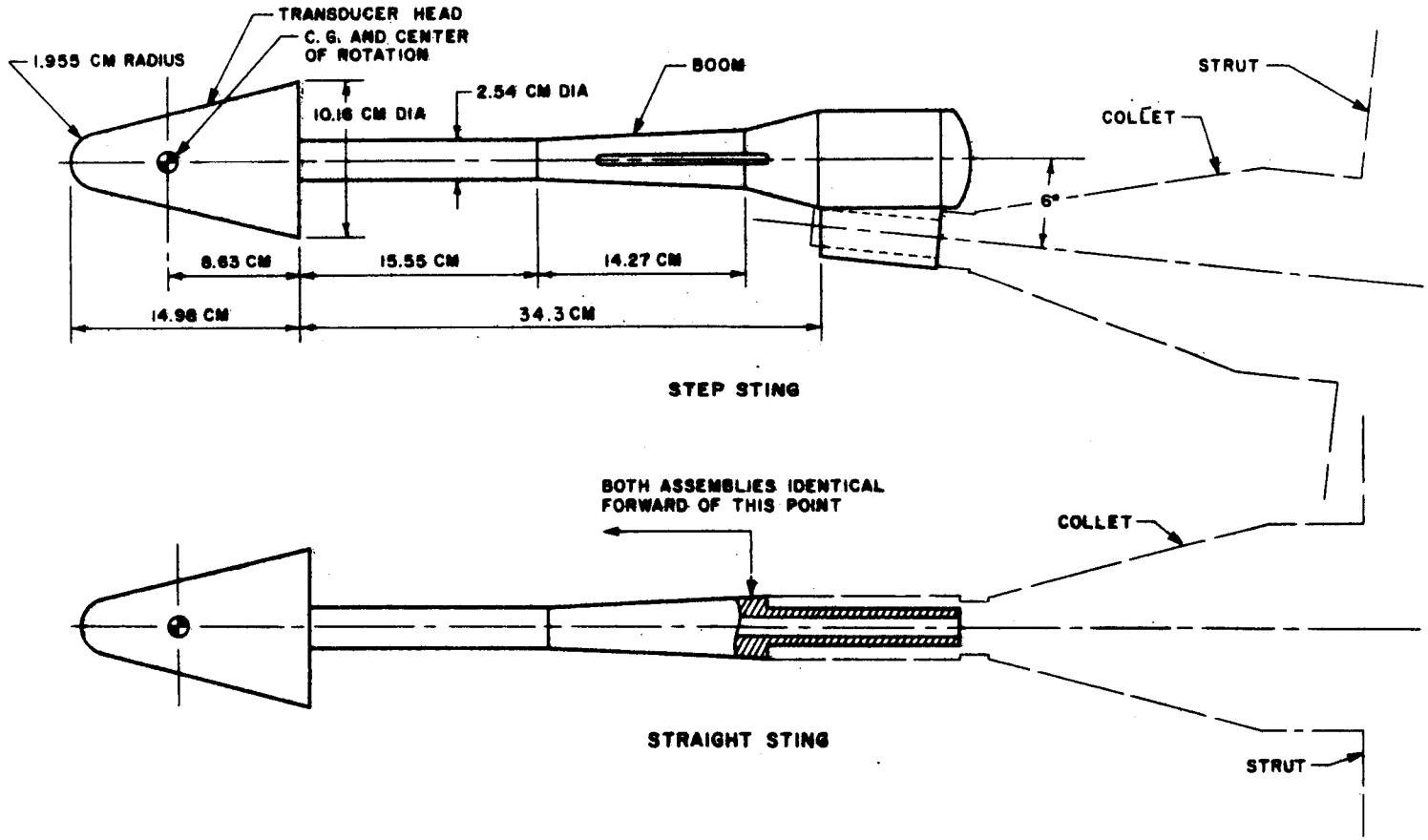

FIGURE 1 OUTLINE OF EDCLIFF 4-15 ANGLE OF PITCH AND YAW TRANSDUCER MOUNTED ON THE TWO STING ASSEMBLIES

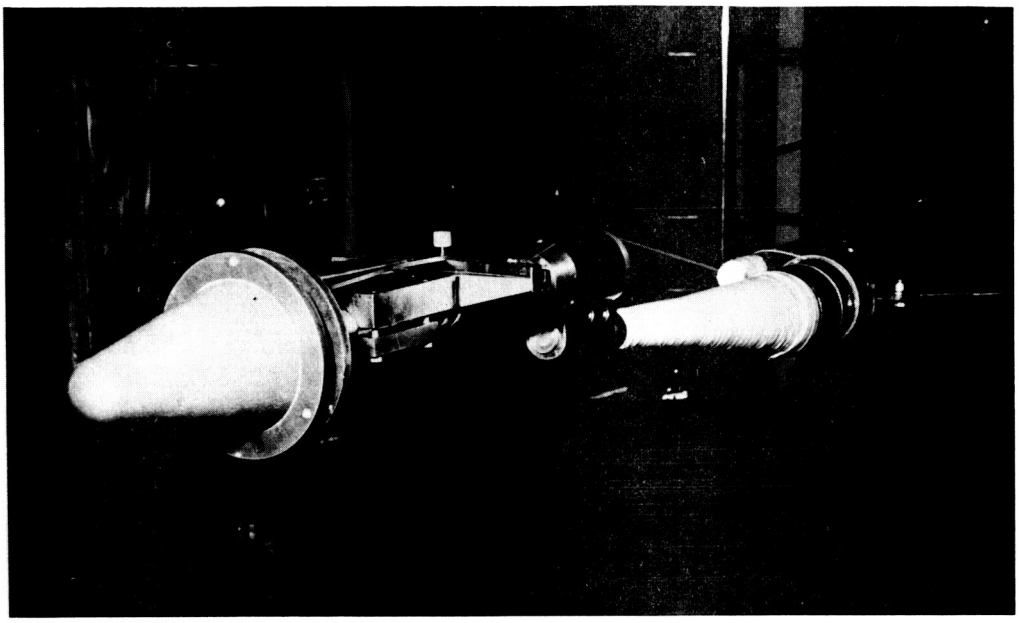

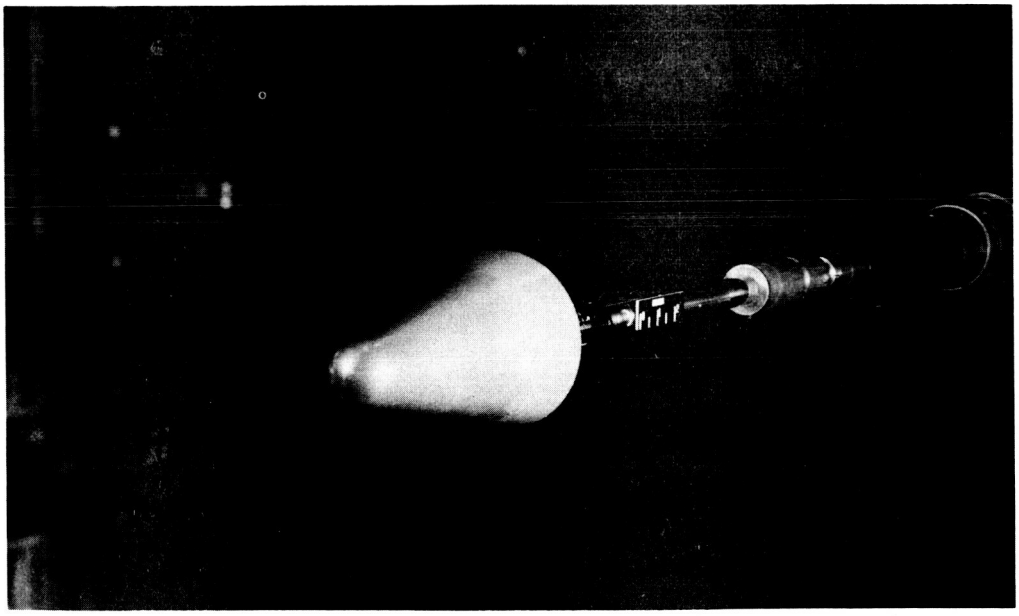

FIGURE 2 PHOTOGRAPHS OF EDCLIFF 4-15 TRANSDUCER MOUNTED IN LRC TUNNEL ON TWO STING ASSEMBLIES (MSFC CALIBRATION FIXTURE VISIBLE IN UPPER PHOTOGRAPH)

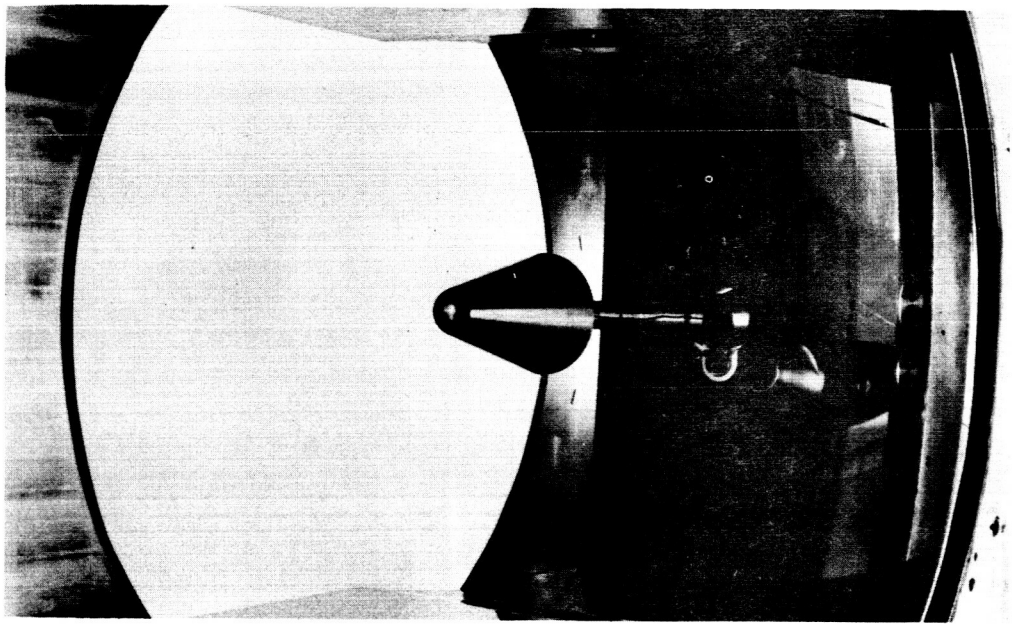

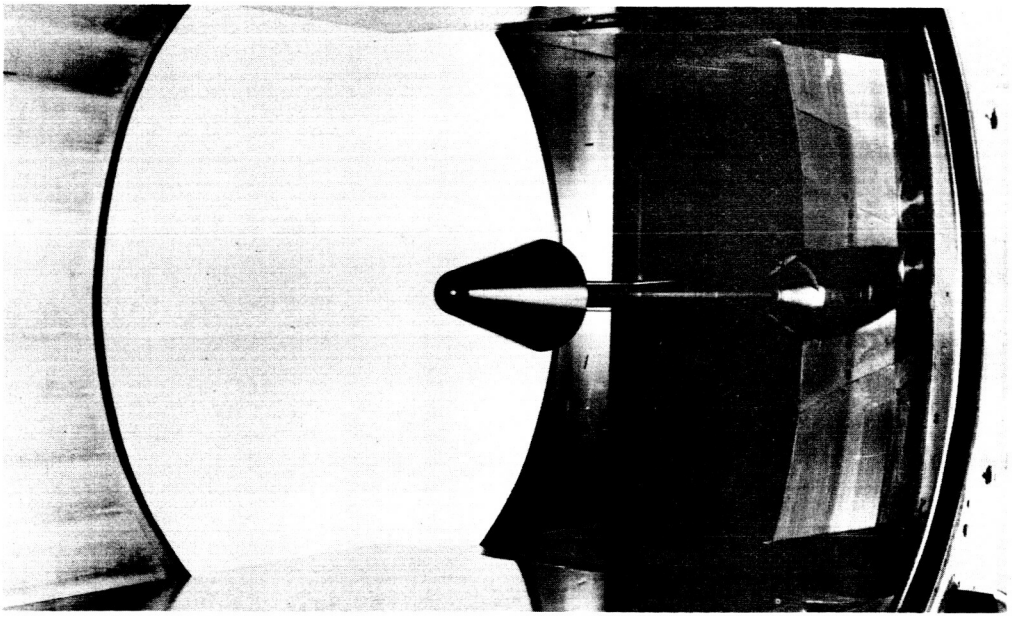

FIGURE 3 PHOTOGRAPHS OF EDCLIFF 4-15 TRANSDUCER MOUNTED IN JPL TUNNEL ON TWO STING ASSEMBLIES

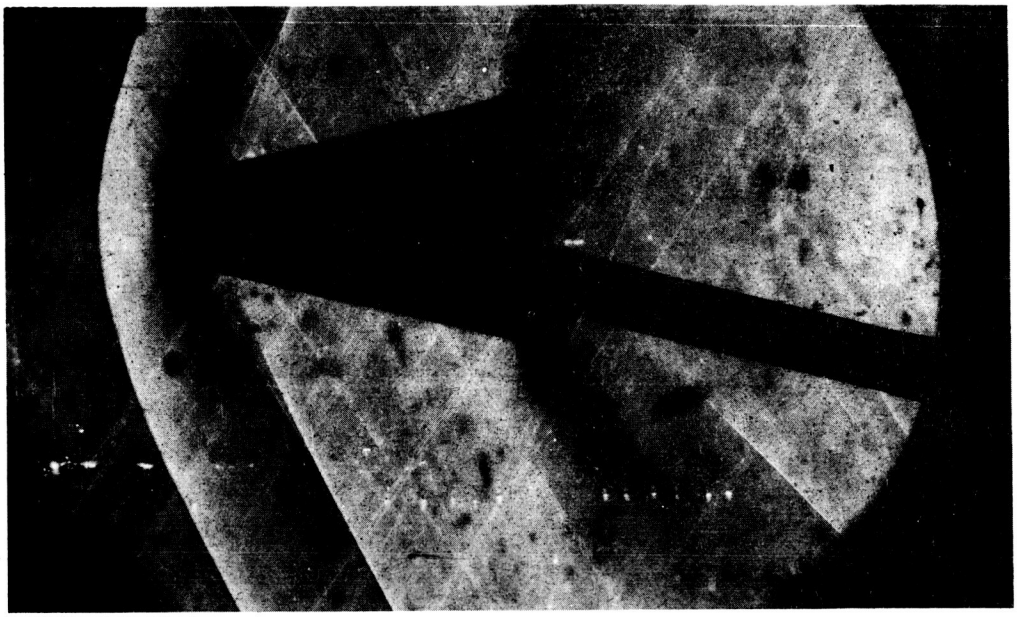

LRC TUNNEL; M=1.2; ANGLE OF PITCH = 13.8 DEGREES

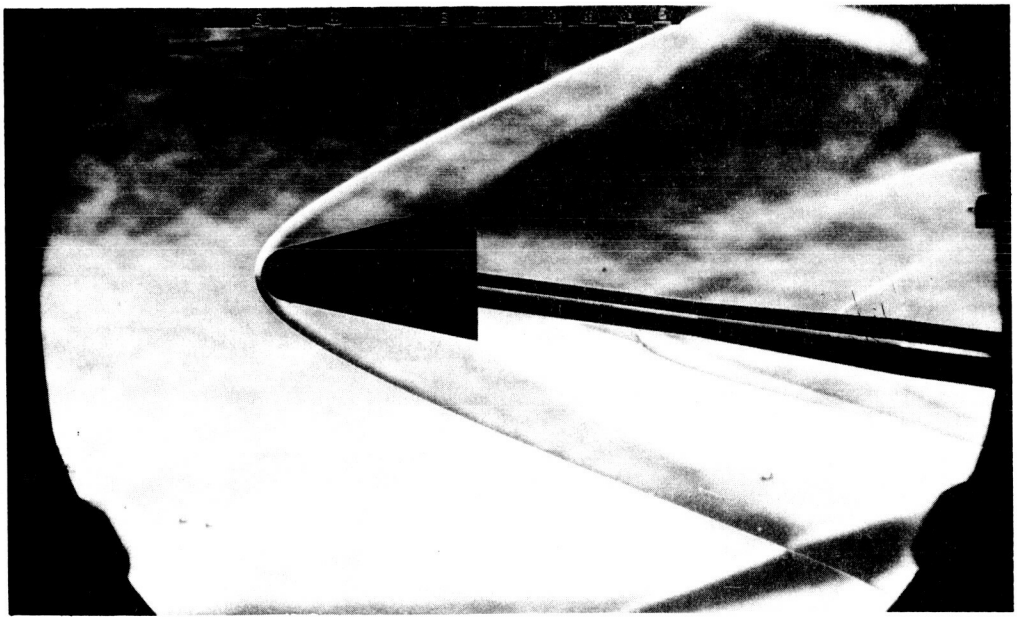

JPL TUNNEL; M=3.01; ANGLE OF PITCH = 9 DEGREES

FIGURE 4 SCHLIEREN PHOTOGRAPHS OF EDCLIFF 4-15 TRANSDUCER IN LRC AND JPL WIND TUNNELS

A static response test at each tunnel condition consisted of reading the output of Transducer P/N 108760-E when the boom was set to various angles with respect to the airflow direction. These tests covered an angular range from minus 9 degrees to plus 14 degrees. Details of the static response of the transducer and notes on appropriate laboratory measurements are presented in Section III.

The dynamic characteristics of Transducer P/N 108760-E were determined in terms of a pure second order system. The objectives of a series of dynamic tests conducted in the wind tunnels were the measurement of natural frequency; damping ratio (fraction of critical damping); and the damping parameter, $2\zeta\omega_n$. The dynamic response was investigated by applying a 3-degree step change in angle of pitch at each tunnel condition. The transducer outputs were recorded on an oscillograph. Dynamic tests were run on both the pitch and yaw axes. Details of the dynamic response data are included in Section IV, which also contains correlations of the data with the corresponding laboratory measurements.

After the wind tunnel tests were performed, Transducer S/N 119 was subjected to environmental tests performed by MSFC. The environmental conditions for these tests were outlined in MSFC Astrionics Division report ASTR-TSR-62, dated 11 May 1962. The results of environmental tests are presented in MSFC Quality Division report, M-Qual-QP-32.

The tests were conducted and the report written for the George C. Marshall Space Flight Center (MSFC), Huntsville, Alabama, by G. R. Mills and J. S. Lukesh of the Air Data Systems Development Unit in the Attitude Control Systems Group of Nortronics, A Division of Northrop Corporation. The MSFC Technical Supervisor and the Responsible Engineer for the program were, respectively, John P. Baur and Bobby S. Gilbert, both of the Aeroballistics Division.

SECTION II. WIND TUNNEL CONDITIONS

Figure 5 is a graph of the trajectory characteristics that were used to establish the wind tunnel testing conditions. The curves were computed for a typical liquid-fueled booster ascent trajectory, which specified altitude, velocity, and dynamic pressure as a function of time. Mach number and Reynolds number were computed using the free-stream temperature at specific altitudes, as given by the 1959 ARDC standard atmosphere (Reference 3). The isentropic total pressure was computed using the standard tables (Reference 4). The characteristics were then crossplotted with respect to Mach number in Figure 5.

Figure 6 is a graphic presentation of the wind tunnel conditions actually achieved. The data points indicate the dynamic pressure, velocity, and Reynolds number versus Mach number conditions. (The data were reduced from the direct measurements of total pressure and total temperature in the tunnel.) The solid curves shown in Figure 6 are the objective trajectory conditions from Figure 5. The data points, which indicate that excellent pressure simulation was achieved, are averages of the measurements made during the dynamic tests. In both the static and dynamic tests, the pressures did not vary from the indicated values by more than one percent; typically the pressure level was held closer than 0.5 percent. Simulation of velocity and Reynolds number above Mach 2 was not attempted. At this time, the only apparent effect of either velocity or Reynolds number was on aerodynamic damping, which is relatively small (see discussion in Section IV B).

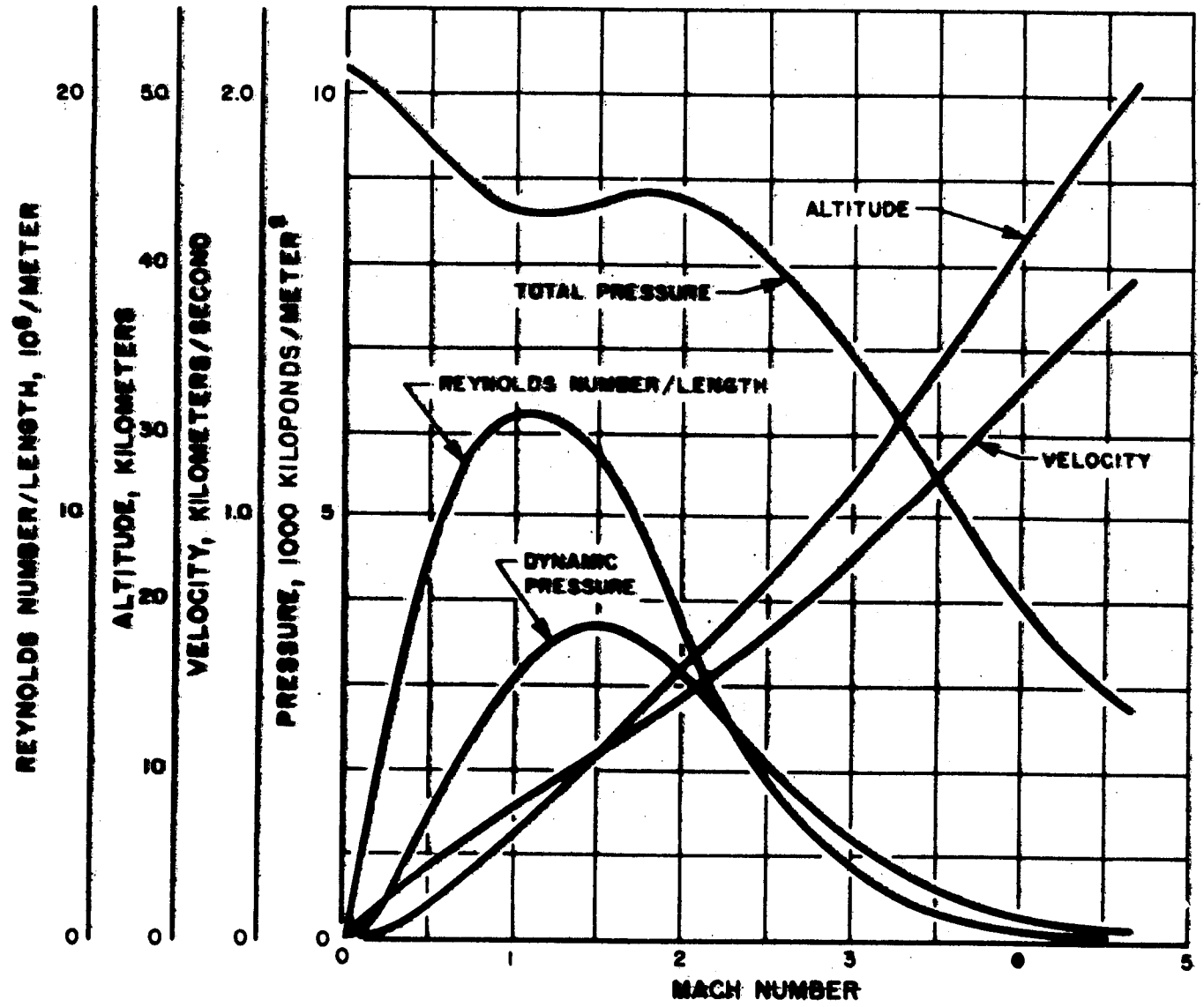

FIGURE 5 CHARACTERISTICS OF A TYPICAL TRAJECTORY OF A LIQUID PROPELLED BOOSTER

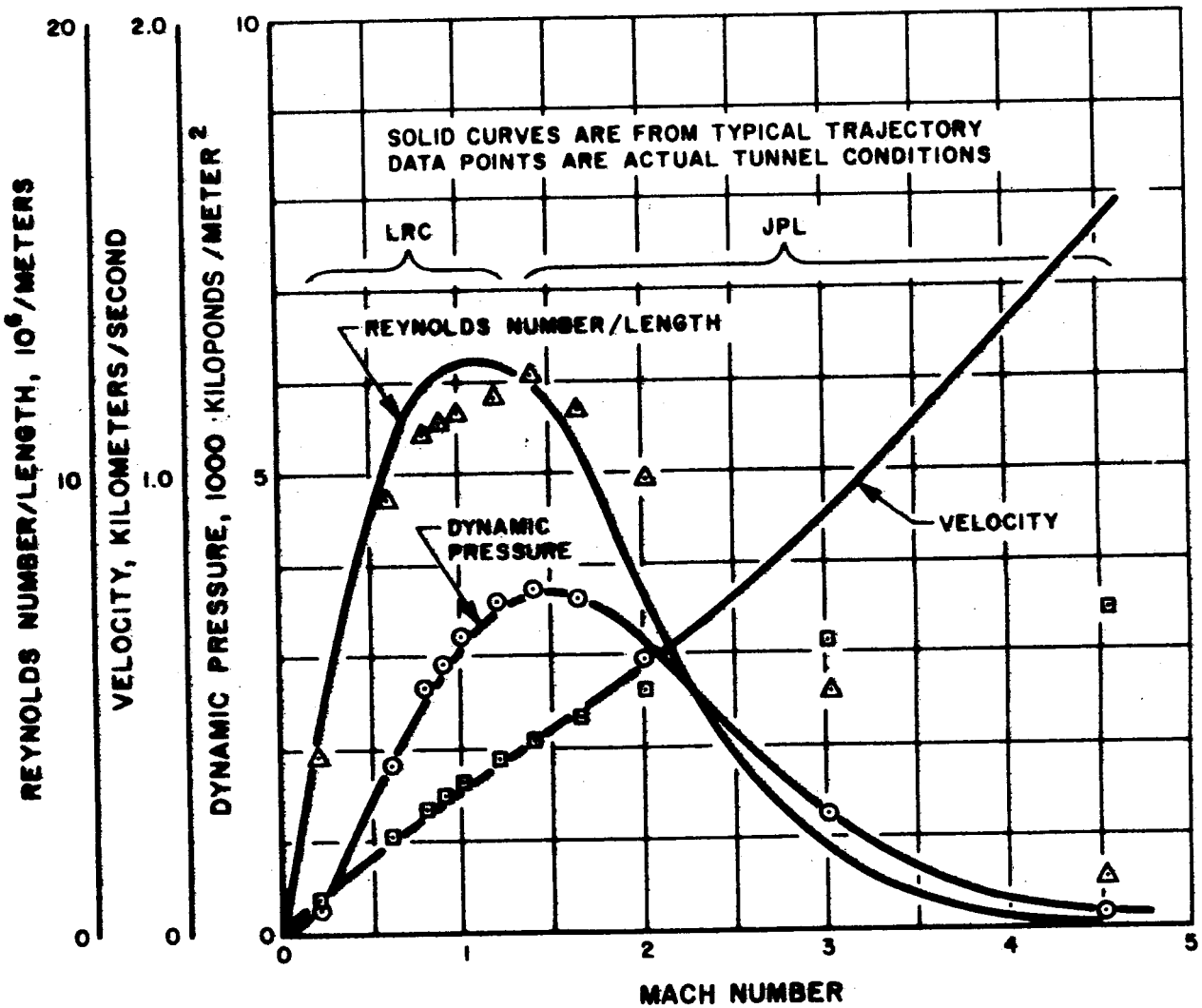

FIGURE 6 WIND TUNNEL CONDITIONS

SECTION III. STATIC RESPONSE CHARACTERISTICS

As a result of the static laboratory and wind tunnel tests, sufficient information exists to correlate future flight measurements. No additional wind tunnel tests are required. This section includes a presentation of all available zero-stability information. The greatest apparent cause of zero shift is potentiometer shift, a characteristic that may be better or worse on other transducers. Potentiometer stability for a specific transducer can be measured in the laboratory. The static response at finite angles of pitch is presented in graphical and tabular form. In both cases, the transducer-indicated output is given as a function of true angle of pitch for each of the Mach numbers in the tests.

A. PRELIMINARY LABORATORY MEASUREMENTS

Prior to the wind tunnel tests, laboratory measurements were made on Transducer Serial Numbers 118 and 119 to establish their suitability for the program.

Zero stability with respect to temperature was determined by comparing electrical-mechanical calibrations made with the transducers at 70° F and 150° F. The movable heads were set at various angles with respect to the boom, using a calibration fixture supplied by MSFC. The calibration fixture is shown mounted on the transducer in one of the photographs in Figure 2. The transducer outputs were read as the position of a 10-turn, 0.05-percent linearity, 20-K, Model A Helipot, nulled in a bridge with the transducer potentiometers. The temperature was measured with a thermocouple mounted on the cover of the aft potentiometer in the transducer.

The output of Transducer S/N 119 was affected by temperature. At a set input angle, the indicated output for the angle of pitch axis was increased by 0.19 degree when the temperature was raised to 150° F. At a set input angle, the indicated output of the yaw axis was increased by 0.05 degree. The slopes of the calibration curves were not affected by temperature. There was no measurable change with temperature on the output of Transducer S/N 118.

Before attempting to perform mechanical-electrical calibration, the mechanical accuracy of the calibration fixture was measured. It is accurate to ±0.03 degree. Prior to each calibration, the fixture was aligned in roll by removing "cross talk." For example, to align the fixture for calibration of the pitch axis, the head was rotated in pitch through ±15 degrees, and the yaw output was measured and reduced to less than ±0.11 degree by adjusting the roll position of the fixture. This corresponds to a fixture roll-position error of 0.11/15 radian or 0.42 degree. The 0.42-degree roll error results in an angle-of-pitch calibration error of less than 0.05 degree.

Since the individual potentiometers were changed during the tests, the potentiometer stability with respect to temperature data cited above are considered typical of what is to be expected; the data are not used in specific interpretation of the JPL tests.

Mass unbalance and starting friction were measured in the laboratory with the transducer in both the horizontal and vertical positions. The average of the absolute values of the torques required to start motion of the head with respect to the boom was used as a measure of starting friction. The difference between the absolute values of the starting torques was an indication of mass unbalance. For both transducers the horizontal mass unbalance was measured as zero, with a measurement accuracy corresponding to an uncertainty of ±1.7 gram-centimeters torque at one gravity. Taken as a possible mass unbalance error, this uncertainty will result in the greatest angular error in the test at Mach 4.54, when the aerodynamic centering torque was lowest; the effect is an angle-of-attack error of ±0.017 degree.

In actual flight, vertical mass unbalance is the significant parameter; the resultant angular error would be proportional to vehicle acceleration. A mass unbalance corresponding to 2.16 gram-centimeters torque at one gravity was measured in the vertical direction for the yaw axis of Transducer S/N 118. (The mass unbalance was zero on both axes of Transducer S/N 119.) For a specific trajectory, the effect of this unbalance plus the measurement error can be computed using the aerodynamic torque relationship presented in Section IV.

The torque required to overcome starting friction in the horizontal position for both axes of Transducer S/N 118 was 8.7 gram-centimeters. For both axes of Transducer S/N 119, 4.3 gram-centimeters was required. These values correspond to the greatest angular error in tests at Mach 4.54, which were 0.085 and 0.043 degree, respectively, for Transducer S/N 118 and S/N 119.

B. ZERO SHIFT

The static wind tunnel tests consisted of positioning the boom to measured (set) angle-of-pitch positions and recording the transducer outputs. The recorded transducer outputs were reduced to indicated angular outputs using electrical-mechanical calibration curves; thus, any transducer potentiometer nonlinearities or initial misalignments were removed from the data. This is desirable because linearity can be independently measured in the laboratory. An output-versus-set-input curve results from the data; typically, the curve does not go through zero. The effect is referred to as a zero shift, which could have a number of possible causes that are grouped in three categories: random, flow direction, and asymmetry.

To isolate the causes of zero error in the static response data, some of the tests were repeated with the transducer rolled 180 degrees. With the resultant information, it is possible to separate the flow-direction type of causes from the asymmetrical causes. (This separation will be referred to hereafter as the 180-degree technique.) However, the random causes will remain in both sets of data. In the following paragraphs are discussed the specific possible causes of zero shift that fall into the three categories mentioned (random, flow direction, and asymmetry).

1. Random Causes of Zero Shift. There are five random errors that could possibly cause a zero shift.

a. Calibration error. Using the calibration fixture supplied by MSFC, calibrations were performed before and after the tests each day and after each model configuration change. The transducer outputs were measured three ways: using the nulled 10-turn calibration potentiometer; using a digital printer readout (wind tunnel equipment) that recorded a voltage off the transducer potentiometer wiper; and by means of an oscillograph that recorded a voltage off the wiper. All the wind tunnel data were subsequently reduced using the printer outputs. As indicated previously, the mechanical calibration fixture is accurate to within ±0.03 degree, and it is positioned in roll such that there is less than ±0.05-degree calibration error.

b. Static friction. Static friction, as indicated previously, corresponds to a starting torque of 8.7 gram-centimeters and 4.3 gram-centimeters, respectively, for Transducers S/N 118 and 119. A consideration that is discussed later in this section excludes from this zero-shift analysis all data of Transducer S/N 118; therefore, the torque value of 4.3 gram-centimeters is used. At Mach 4.54, the aerodynamic centering torque was least, therefore the angular error caused by static friction was greatest. The effect was 0.043 degree at this Mach number. Vibration, however, probably reduced the effect during the static response tests.

c. Variations in the characteristics of the transducer readout equipment. A comparison of the printer records and the calibration potentiometer readings confirmed printer accuracy. All readings were consistent within 0.04 degree; they were typically within 0.02 degree of each other.

d. Random flow variation due to turbulence. Turbulence in the tunnels caused random variations in the transducer output. The oscillograph records indicate the effect of the turbulence to be as great as a ±0.15-degree variation from the mean. The printer systems included dampers that served to smooth out turbulences in the printer readings.

e. Shift in the transducer potentiometer position. Comparisons of calibrations made before and after wind tunnel tests indicated shifts in the transducer zero reading of up to 0.18 degree. Considering the precision of the calibration procedure, differences of this magnitude can only be interpreted as representing actual changes in the transducer potentiometer position.

2. Flow Direction Causes of Zero Shift. Although some of the random zero-shift causes listed above are substantial, it is still appropriate to attempt separation of the flow-direction type zero-shift causes from those resulting from aerodynamic asymmetry. As stated, this will be done by a procedure described as the 180-degree technique. To make the separation, it must be assumed that there is no day-to-day flow-direction variation in the tunnel, because the tests performed with the transducer rolled 180 degrees were never run on the same day as the zero-roll tests. The flow-direction causes of zero-shift are of four types.

a. Deviation of the actual wind tunnel flow from the stated direction may cause a zero shift.

b. A sting fixture that is not straight changes the effective direction.

c. Mass unbalance of the transducer may result in a zero shift. The effect of mass unbalance is measurable in the laboratory; it is less than ±0.017 degree for both transducers (see Section III A). Therefore, it is of no concern that the effect is lumped with the flow-direction causes in the reduction of the wind tunnel data.

d. A zero shift may occur because of downstream sting geometry.

The combined effects of the flow-direction-type causes in some cases constituted a significant zero shift; at Mach 2.01 (JPL tunnel) the shift was 0.6 degree.

3. Asymmetrical Causes of Zero Shift. The asymmetry category of zero shift causes includes any physical characteristic of the transducer that would cause the line through the aerodynamic center of pressure and the center of rotation to be other than perpendicular to the plane of the transducer base.

Figure 7 is a plot of the apparent effect of asymmetry on zero shift for Transducer S/N 119. All the data have been corrected for the effects of flow direction errors; however, the effects of random errors remain. For reference, the magnitudes of the potentiometer-shift effect and the calibration-accuracy effect are also shown in Figure 7. If all the random causes of the zero shift are indeed random, it is possible to attribute the consistently low zero reading to asymmetrical aerodynamics of Transducer 119. The average reading is minus 0.05 degree; however, there is not enough data for this to be considered conclusive.

The data plotted in Figure 7 include only the reduced zero points for which the corresponding 180-degree test was performed, using the same sting. No similar chart exists for Transducer S/N 118 because 180-degree tests were not performed with the same sting. In all tests at Mach numbers greater than 1.40 (JPL tests), Transducer S/N 119 was tested with both stings. However, 180-degree tests were performed using only the straight sting. An attempt to apply the flow-direction correction determined using the straight sting to the step-sting data was not successful. Figure 8 is a presentation of the zero error remaining for both the step and straight sting data if the correction is made. The conclusion drawn was: either one of the stings was not straight, or the flow direction was affected by the sting geometry, even though the tests were conducted at Mach numbers greater than 1 and the asymmetry in the step sting begins 34 centimeters from the rear of the transducer head. Apparently, the step sting increases the angle of pitch. The average difference is +0.23 degree. It is concluded that the flow-direction correction can be considered as determined only in those cases in which the 180-degree tests were conducted with the same sting. All those cases are represented in Figure 7.

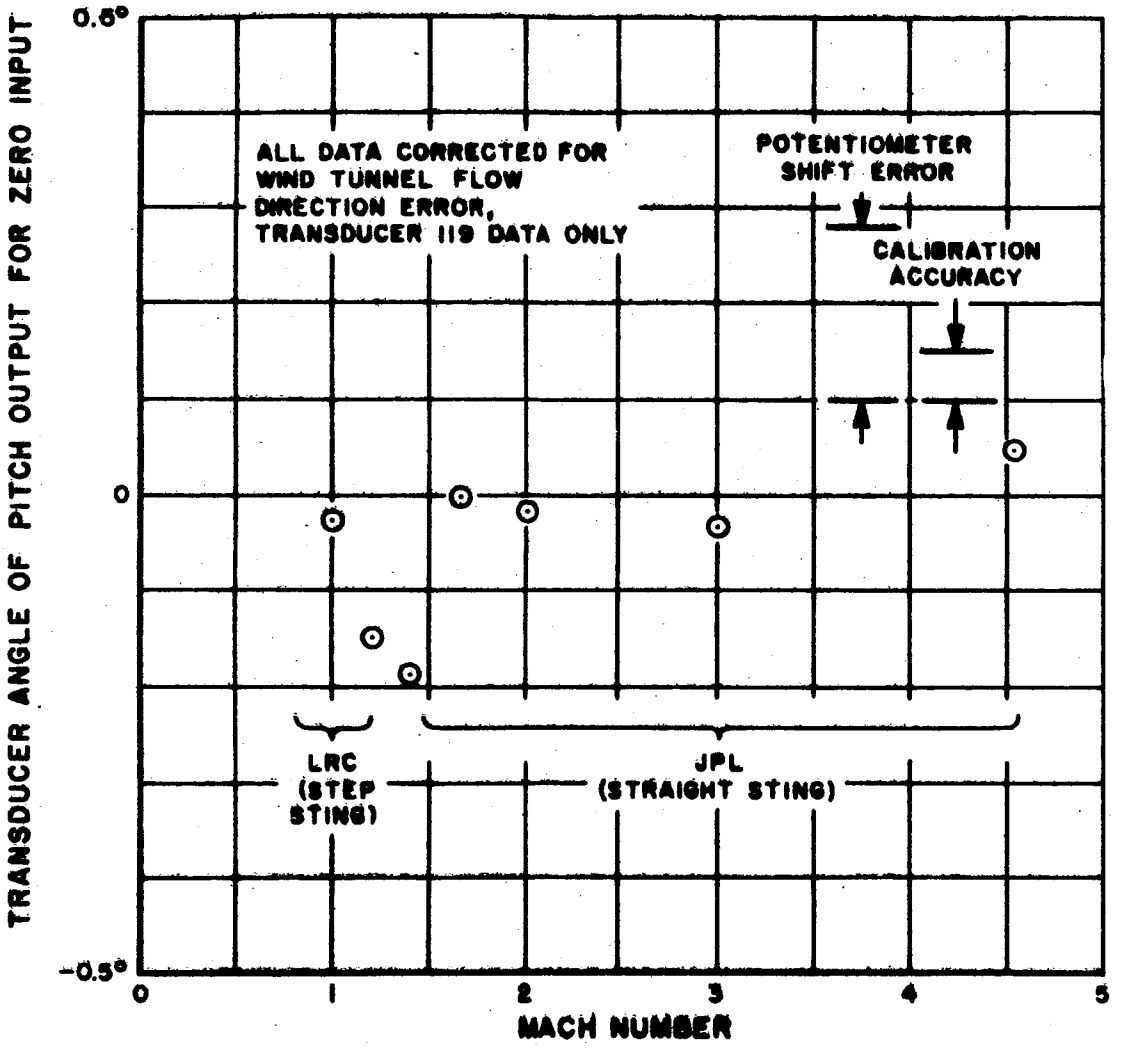

FIGURE 7 ZERO SHIFT CAUSED BY GEOMETRICAL ASYMMETRY ON PITCH AXIS OF TRANSDUCER S/N 119

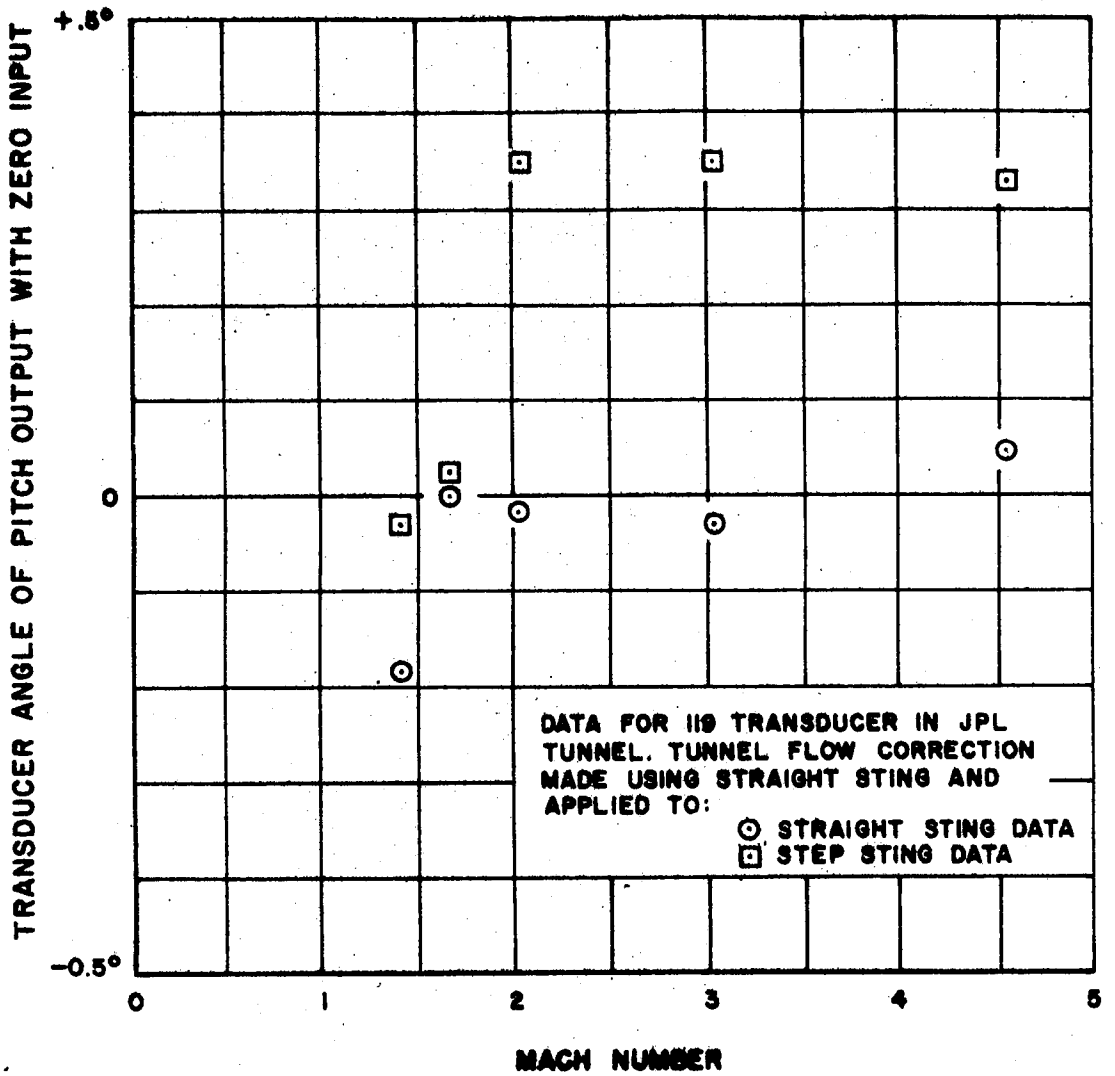

FIGURE 8 APPARENT GEOMETRICAL ASYMMETRY USING BOTH STRAIGHT AND STEP-STING DATA

C. STATIC ANGLE OF ATTACK RESPONSE

In Section III B, all conclusions that can be made both from the available laboratory and wind tunnel data regarding zero shift or static-bias error were discussed. It is appropriate at this point to consider the static response of the transducer at finite angles of pitch exclusive of zero shift from any source.

For each static response run, all the wind tunnel data have been reduced with the input axis shifted so that the best curve through all the data goes through zero. Because the zero error is removed, it is possible to include data from tests for which there were no corresponding 180-degree-roll tests; this includes tests made with Transducer S/N 118 and tests on the yaw axis of Transducer S/N 119.

During the tests at LRC, it was noted that the curves of output versus input were assuming an "S" shape at various Mach numbers. The first tests used the step sting, which was suspected as the cause of the "S" shape. The step sting was replaced with a straight sting, but the "S" shape remained; however, it was discovered at the end of the straight-sting test runs that part of this assembly had come loose, allowing a movement of ±0.25 degree. It could not be determined with certainty when this occurred; therefore, all the LRC straight sting static response data have been discarded.

Figures 9 and 10 are graphs in which are summarized all the static response data, except those instances when yaw angle was not zero. Included are data from tests using both transducers, both sting configurations (at JPL), and both axes of Transducer S/N 119. The dashed lines are reference lines that have slopes of unity. Excellent repeatability was achieved in the data taken under these various conditions. The "S" shape is apparent at Mach numbers near 1.

Figure 11 is a plot as a function of Mach number of the effective transducer gain about zero. The points in Figure 11 are the slopes about zero of the best curves that fit the static response data in Figures 9 and 10 at the various Mach numbers.

Table 1 presents in tabular form the indicated angle of pitch as a function of true input angle of pitch and Mach number. The tabulated data represent the consensus of the wind tunnel tests. The tabulations are interpolated from the best smooth curves that can be inscribed through the static response points shown in Figures 9 and 10.

At all conditions greater than Mach 1.40, static response tests were run on the angle-of-pitch axis of Transducer S/N 118, with the angle of yaw at 6 degrees. As shown in Figure 12 all the data have been shifted on the input axis so that the best curve goes through zero. The solid curves shown in Figure 12 are reference lines prepared from the zero yaw data plotted in Figure 10; that is, the solid curves in Figure 12 are the best fit to the Figure 10 data. With the transducer at an angle of yaw of 6 degrees, the static response is remarkably close to that with zero yaw.

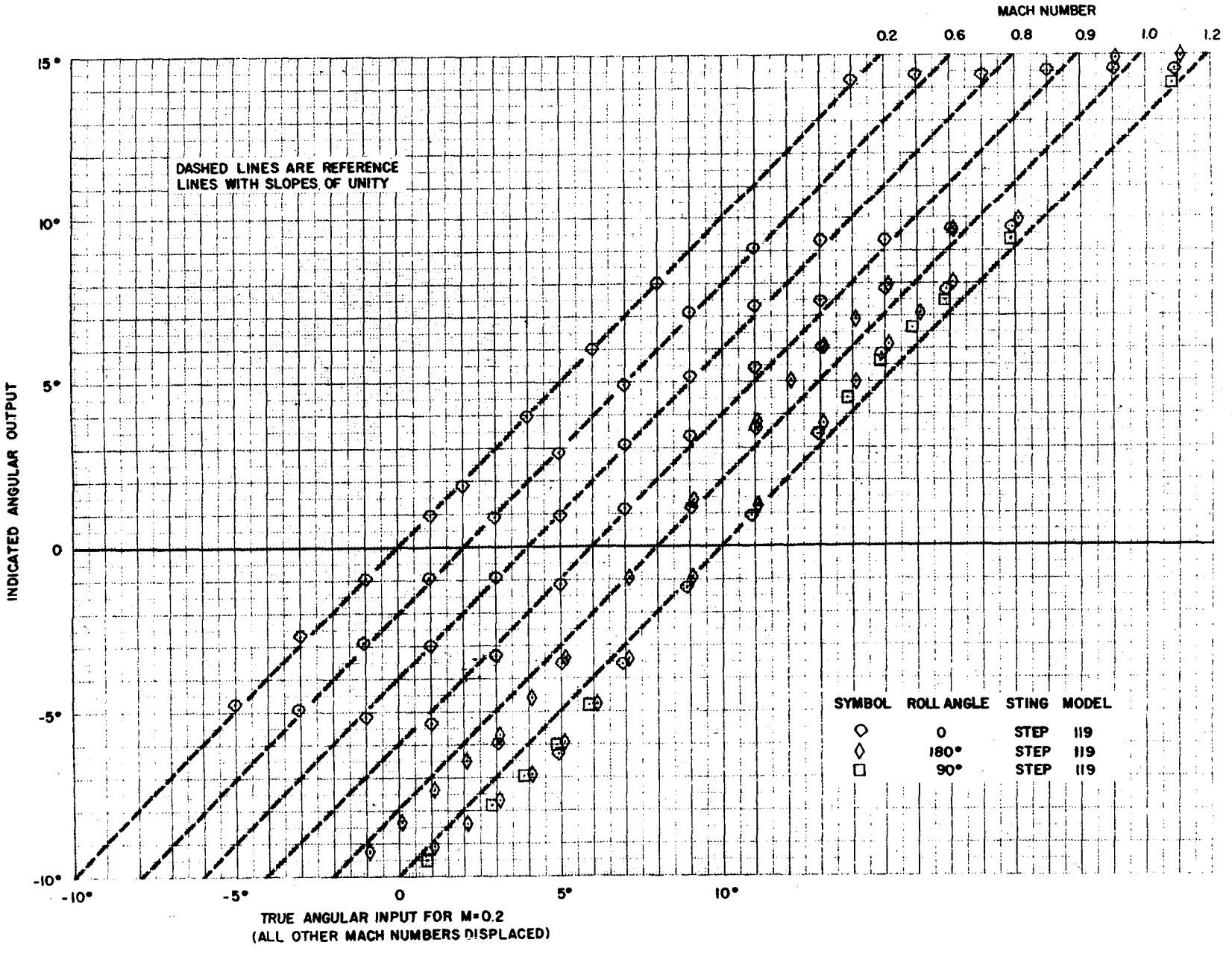

FIGURE 9 ZERO CORRECTED STATIC RESPONSE DATA, LRC TUNNEL

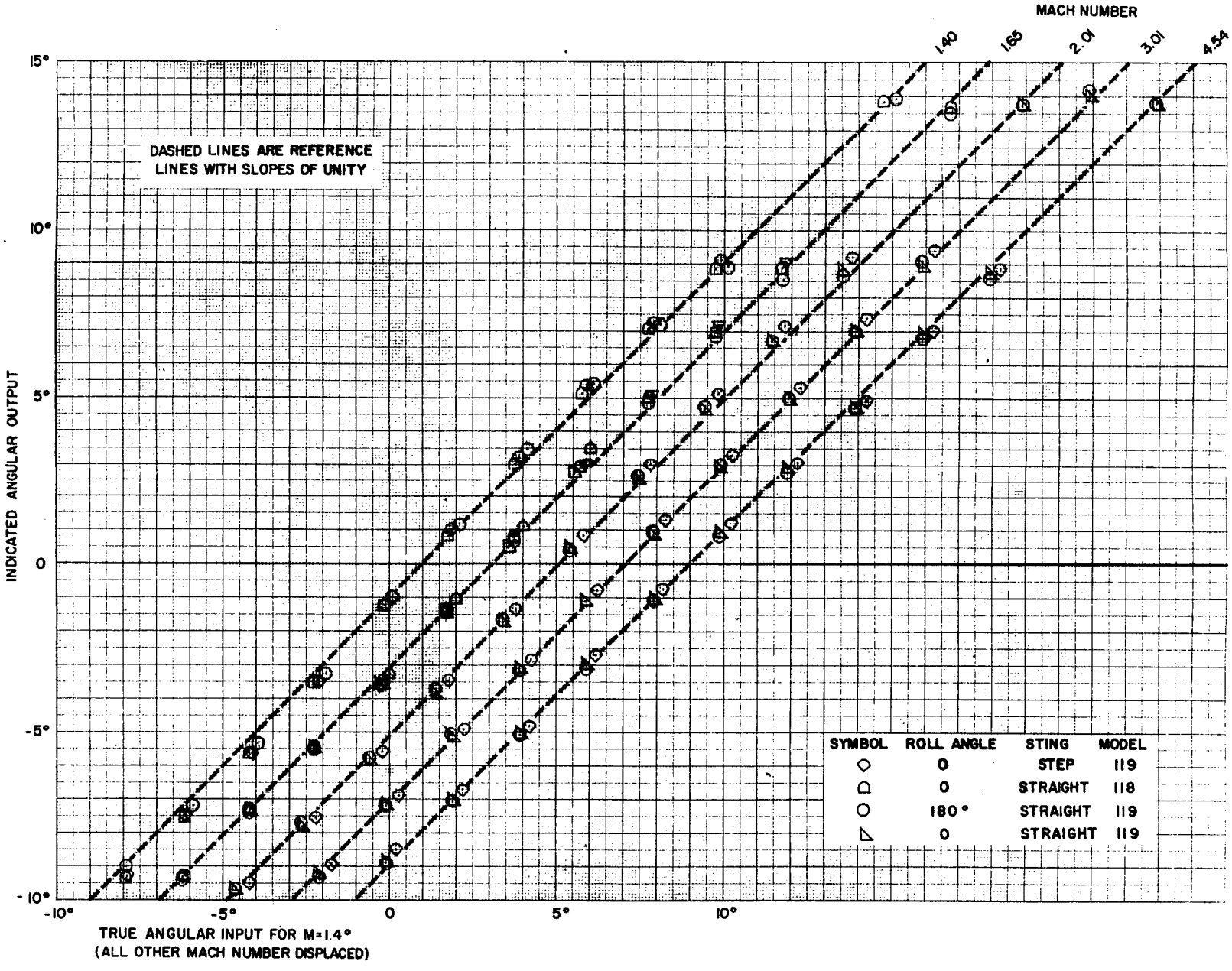

FIGURE 10 ZERO CORRECTED STATIC RESPONSE DATA, JPL TUNNEL

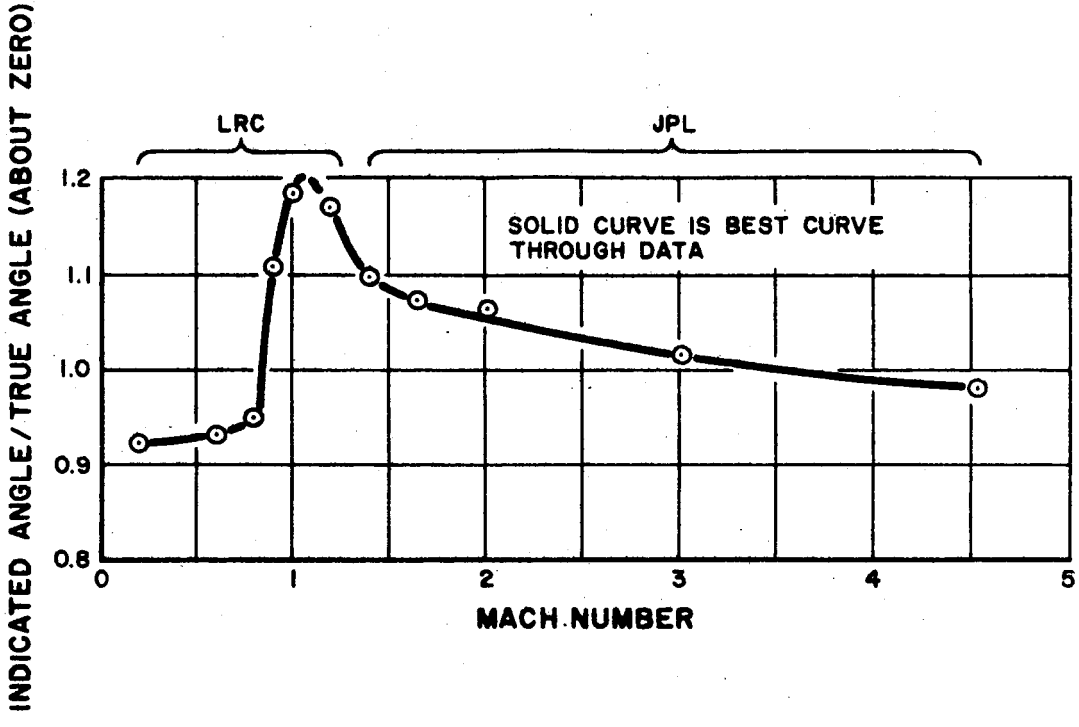

FIGURE 11 SLOPE (ABOUT ZERO) OF STATIC OUTPUT ANGLE WITH RESPECT TO SET INPUT ANGLE

TABLE 1 INDICATED ANGULAR OUTPUTS AS A FUNCTION OF TRUE ANGLE AND MACH NUMBER

Indicated Angular Output (degrees) / True Angular Input (degrees)	Mach Number 0.2	0.6	0.8	0.9	1.0	1.2	1.40	1.65	2.01	3.01	4.54
1	0.92	0.93	0.95	1.11	1.19	1.17	1.10	1.07	1.06	1.02	0.98
2	1.85	1.87	1.96	2.22	2.38	2.39	2.20	2.15	2.13	2.03	1.96
3	2.80	2.85	3.01	3.33	3.56	3.52	3.30	3.22	3.19	3.05	2.94
4	3.80	3.86	4.08	4.39	4.75	4.69	4.39	4.29	4.26	4.07	3.92
5	4.84	4.89	5.16	5.41	5.82	5.86	5.41	5.30	5.32	5.09	4.90
6	5.89	5.99	6.23	6.41	6.79	6.91	6.39	6.24	6.32	6.10	5.88
7	6.94	7.08	7.29	7.42	7.67	7.87	7.32	7.18	7.29	7.12	6.86
8	7.98	8.17	8.32	8.40	8.56	8.74	8.24	8.13	8.25	8.10	7.82
9	9.03	9.26	9.34	9.37	9.50	9.62	9.12	9.07	9.24	9.08	8.74
10	10.07	10.33	10.36	10.33	10.46	10.56	10.05	10.02	10.24	10.09	9.73
11	11.12	11.38	11.38	11.36	11.46	11.52	11.00	10.96	11.25	11.10	10.73
12	12.17	12.41	12.40	12.39	12.50	12.51	12.00	11.90	12.28	12.11	11.74
13	13.22	13.43	13.41	13.44	13.55	13.54	13.00	12.85	13.33	13.13	12.79
14	14.26	14.45	14.42	14.53	14.63	14.59	14.00	13.80	14.38	14.16	13.86

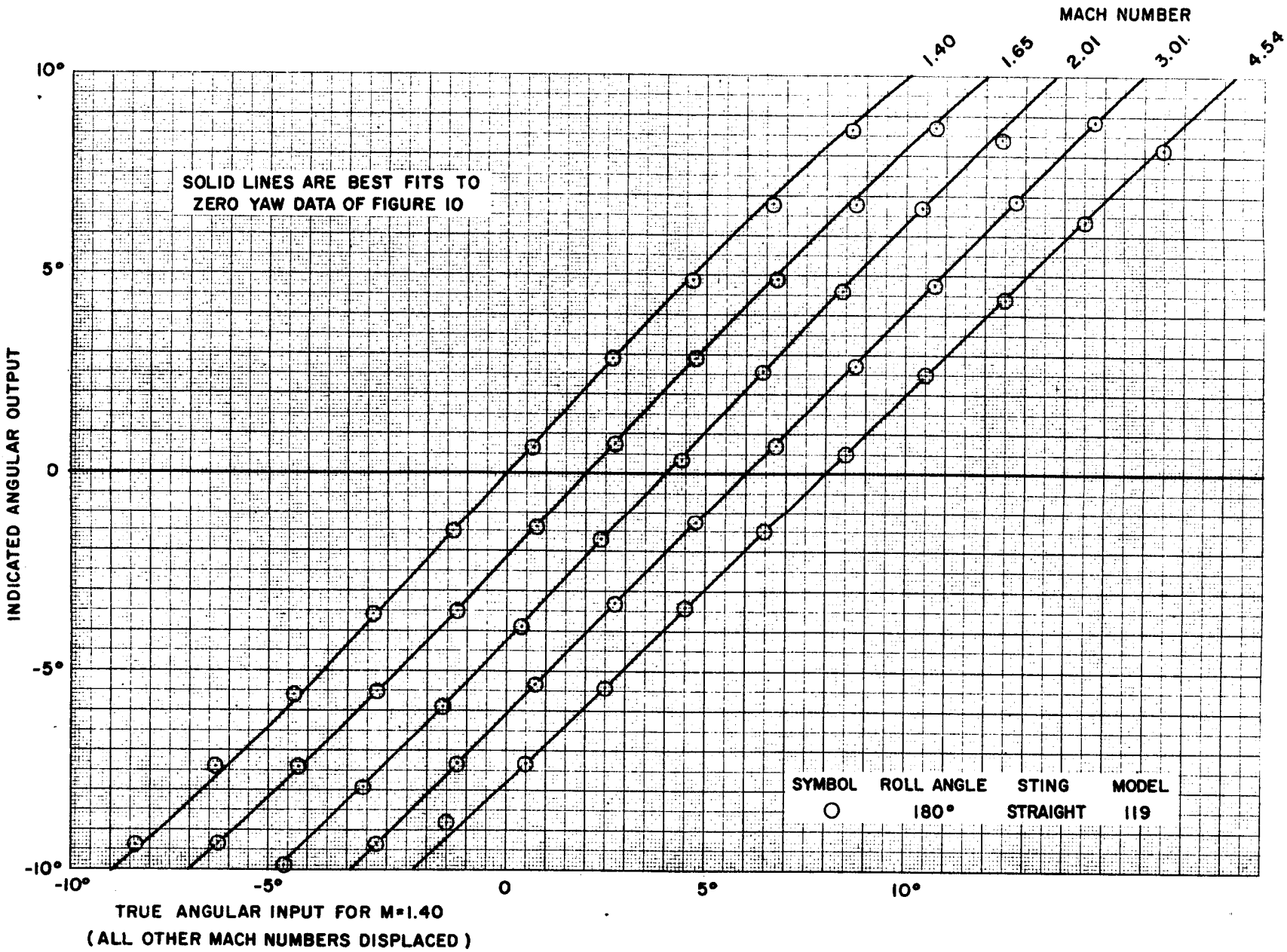

FIGURE 12 ZERO CORRECTED ANGLE OF PITCH STATIC RESPONSE DATA FOR 6-DEGREE ANGLE OF YAW

SECTION IV. DYNAMIC RESPONSE CHARACTERISTICS

A. CALCULATIONS

The static response characteristics presented in Section III should apply to all Edcliff Model 4-15 transducers, because that model number specifies all the geometrical parameters on which the static response characteristics are dependent. The dynamic response characteristics, however, are affected by the head moment of inertia (which depends on the head material) and on the viscous dampers. The tested transducers were identified by P/N 108760-E; the dynamic response characteristics presented in this section apply to transducers of that part number.

While the transducer is in an airstream, there are five primary torques acting in the pitch and yaw directions on the movable head:

1. The aerodynamic centering torque is approximately proportional to the misalignment of the transducer head with the airflow, and is a function of dynamic pressure and Mach number

2. The aerodynamic damping torque is approximately proportional to the angular velocity of the head and is a function of dynamic pressure, velocity, and Mach number

3. The viscous damping torque is approximately proportional to the angular velocity of the head, and is not a function of the trajectory conditions

4. The mass unbalance causes a torque that is a function of the absolute acceleration

5. Friction causes a torque that is constant while rotation exists in one direction.

The characteristics of these five primary torques are discussed in the following paragraphs.

ITEM 1. Aerodynamic Centering Torque. The geometry of the Edcliff 4-5 Angle of Pitch and Yaw Transducer, as specified by MSFC, has aerodynamic characteristics that are well known. For the tests discussed in this report, MSFC supplied: curves of the derivative of the normal force coefficient with respect to angle of pitch about zero, as a function of Mach number; and curves of the center of pressure location at zero angle of pitch as a function of Mach number. These relationships, taken together with the known location of the transducer center of rotation, are sufficient to determine a relationship between an aerodynamic torque coefficient derivative versus Mach number.

The aerodynamic torque is proportional to the transducer scale factor to the power of three (the force is proportional to the base area and the moment arm is proportional to the diameter). To nondimensionalize the torque coefficient derivative, it is defined in terms of the base area to the power of three halves, as follows:

$$\frac{dT}{d\theta}_{\theta=0} = C_{M_\theta} A^{3/2} q \tag{1}$$

where,

$$A^{3/2} = 731 \text{ centimeters}^3$$

At small angles, the torque is equal to the product of $dT/d\theta$ and θ. Figure 13 is a plot of the relationship between C_{M_θ} versus Mach number.

ITEM 2. Aerodynamic Damping Torque. An approximate calculation of the expected aerodynamic damping is next performed. If a body is rotating longitudinally in an airstream, the air at any surface element has a normal component of velocity, due to the rotation, which is approximately equal to

$$V_N = \dot{\theta} X \tag{2}$$

where,

X = distance of surface element from the center of rotation.

The ratio of V_N and the air velocity in the longitudinal direction is an effective angle of pitch, which exists even when the real angle of pitch is zero. The appropriate distance from the center of rotation is chosen as the center of pressure distance. The effective angle of pitch is

$$\frac{V_N}{V} = \frac{\dot{\theta} X}{V} \tag{3}$$

the damping torque is determined using Equation 1.

$$T_d = \frac{V_N}{V} C_{M_\theta} A^{3/2} q = \frac{\dot{\theta} X}{V} C_{M_\theta} A^{3/2} q \tag{4}$$

The torque is indeed a damping torque, because it is proportional to $\dot{\theta}$. The damping torque coefficient, B, is defined as the ratio of the torque and $\dot{\theta}$; therefore,

$$B = \frac{X}{V} C_{M_\theta} A^{3/2} q \tag{5}$$

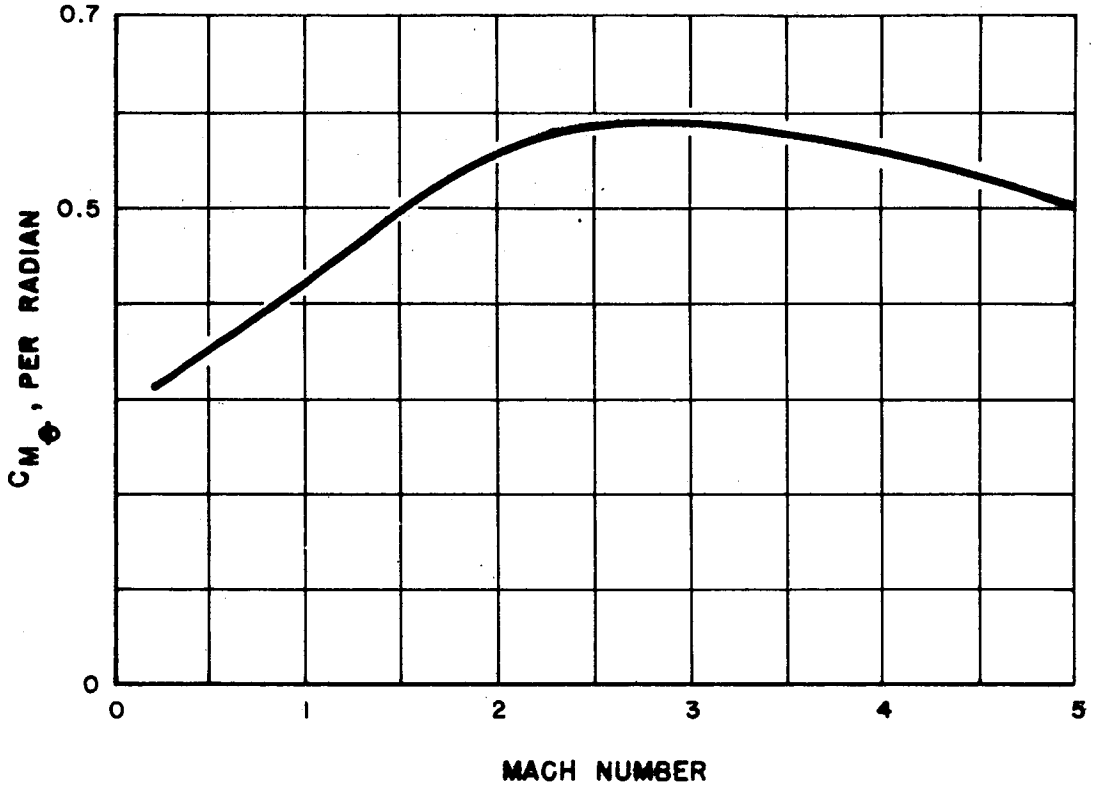

FIGURE 13 TORQUE COEFFICIENT DERIVATIVE COMPUTED FROM PREVIOUSLY ESTABLISHED AERODYNAMICS OF THE TRANSDUCER GEOMETRY

It is appropriate to consider damping in terms of the damping torque coefficient, or the ratio B/I, instead of a damping ratio. (I = 6.71 gram-centimeter-seconds and is the moment of inertia of the transducer head.) Because the viscous damping is predominant (as will be shown), the B or B/I is independent of trajectory conditions, whereas the damping ratio is not.

Figure 14 is a plot of the B/I ratio due to aerodynamic damping. Two sets of information are presented in Figure 14: the solid curve is the aerodynamic damping expected for the typical trajectory shown in Figure 5; the circled points are the computed aerodynamic damping factors that should have been experienced in the wind tunnel tests. They differ because the velocity was not simulated exactly, as shown in Figure 6.

ITEM 3. Viscous Damping Torque. The characteristics of viscous damping torque are discussed in Section IV B, which follows.

ITEMS 4 and 5. Mass Unbalance and Static Friction. The torques resulting from mass unbalance and friction were measured in the laboratory (see discussion in Section III A). Using the torque coefficient derivative plotted in Figure 13, with the trajectory conditions of Mach number and dynamic pressure, the measured torques can be interpreted in terms of an angular error. As stated previously (Section III A), the effects of the two were greatest in the test at Mach 4.54, when the aerodynamic torque was least. At Mach 4.54, the mass unbalance effect is less than ±0.017 degree; the friction effect is less than 0.085 degree.

At a given trajectory condition, the Mach number, dynamic pressure, velocity, and acceleration are fixed. Under these conditions, all the torques fall into three categories, discussed in the following paragraphs.

At small angles, the aerodynamic centering torque is proportional to θ, according to Equation 1.

Aerodynamic damping and viscous damping combine to cause a torque proportional to $\dot{\theta}$.

Mass unbalance and friction are constant torques (the direction of the friction torque is dependent on the direction of θ).

To the extent that the above proportionality relationships exist, a second-order equation of motion results.

$$I\ddot{\theta} + B\dot{\theta} + K\theta = T_{\text{mass unbalance}} \pm T_{\text{friction}} \tag{6}$$

where,

K is $dT/d\theta$ of Equation 1, and

B is the lumped damping coefficient.

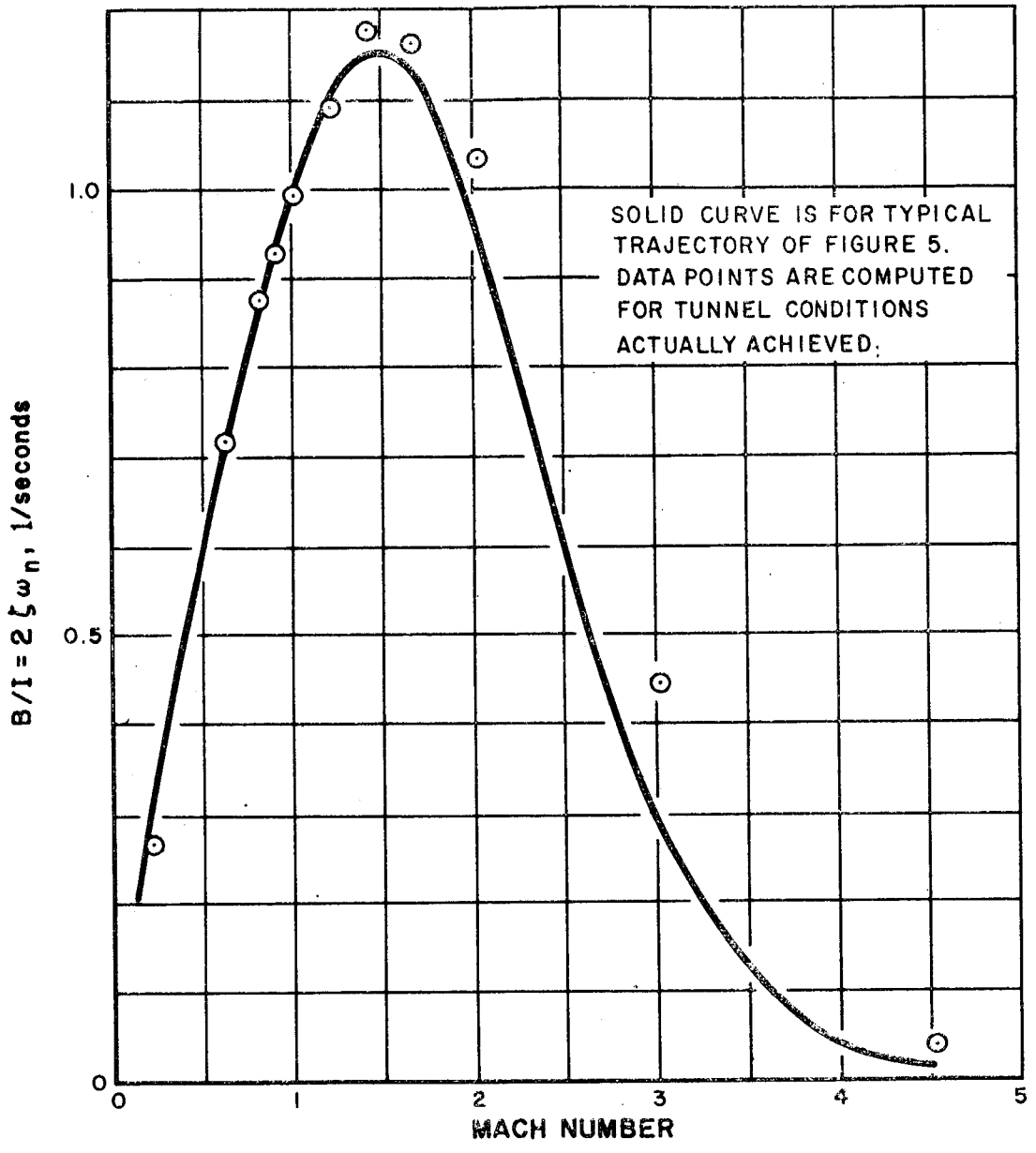

FIGURE 14 AERODYNAMIC DAMPING FACTOR

As has been shown, the mass unbalance and friction torques are small for all test conditions. It is appropriate to consider them to be negligible, in which case a simple homogeneous second-order equation remains. The undamped natural frequency and damping ratio are

$$\omega_n = \sqrt{\frac{K}{I}} \tag{7}$$

$$\zeta = \frac{B}{2I\omega_n} \tag{8}$$

Accordingly, the ratio of the damping coefficient and the moment of inertia is

$$B/I = 2\zeta\omega_n \tag{9}$$

B. PRELIMINARY LABORATORY MEASUREMENTS

Laboratory measurements were made prior to the wind tunnel tests to determine the damping factors due to the viscous damping in the transducer heads. For the LRC tests, two fluid-viscocity values were selected: 30 thousand and 60 thousand centistokes. Transducer S/N 118 used the less-viscous damping fluid. Evaluation of the initial dynamic response data using Transducer S/N 118 in the LRC tests indicated less damping than anticipated; therefore, Transducer S/N 119 was used in all dynamic tests at LRC. Prior to the tests at JPL, the more-viscous fluid was also put into Transducer S/N 118, which was then used as the primary instrument for those tests.

Three methods were used to measure the viscous damping factor in the laboratory.

With the transducer mounted vertically, a known mass was added to the head so that the total center of gravity fell below the center of rotation. To a step change in torque, the transducer then responded as a damped pendulum. Oscillograph records made of the transducer output were reduced graphically in terms of damping factor.

With the transducer mounted vertically, a calibrated centering spring assembly was attached to the head. To a step change in torque, the transducer responded as an almost pure second-order system. The output was recorded on an oscillograph and the damping factor was determined.

With the transducer mounted horizontally, a known step torque was applied by means of a weight. The time response to the change in torque was recorded on an oscillograph and reduced in terms of the damping factor.

The three measurement methods described were required because the damping factor was not constant but was a function of the effective angular velocity of the head (Reference 5 discusses this phenomenon). The three measurement methods resulted in progressively greater angular velocities.

Because the damping factor is also a function of the transducer temperature, tests were run at three temperatures: 70° F, 115° F, and 150° F. Figure 15 includes all the damping data taken for Transducer S/N 119 prior to the LRC tests. The data is plotted in terms of the B/I damping factor. Note that the aerodynamic damping (shown in Figure 14), at the maximum, is two orders of magnitude less than the viscous damping. The damping factors are plotted in Figure 15 with respect to temperature (which was measured with the thermocouple in the head), and angular velocity. In the cases of the tests that yielded oscillatory oscillograph records, the angular velocity was measured as the slope of the straight line drawn through the first two peaks (positive and negative peaks); the slope is equivalent to the average velocity. The horizontal method yielded traces that approached straight lines, the slopes of which were used as the velocities.

C. TEST RESULTS

The dynamic response of the transducer was measured at each wind tunnel condition by physically offsetting the head approximately three degrees, using a special trip mechanism that had an instantaneous trip. (Had the deviation from the instantaneous condition been significant with respect to this investigation, the deviation would have been clearly evident on the oscillograph records; no deviation from the instantaneous condition was apparent.) Oscillograph records of the transducer output were used to observe the dynamic behavior.

Figure 16 is a typical oscillograph trace. The response is interpreted in terms of that of a pure second-order system as indicated by Equation 6. Graphical measurements were used to determine the undamped natural frequency, ω_n, the damping ratio, ζ, and the average head angular velocity for each dynamic record. All data for each tunnel condition have been averaged.

Figure 17 is a graphical representation of the average at each wind tunnel condition of the undamped natural frequency (converted from the direct measurement of the damped natural frequency) and the damping ratio. The solid curves shown in Figure 17 are the best curves through the data.

It has been shown that the aerodynamic damping is small with respect to the viscous damping. Therefore, the total B/I damping factor should be essentially independent from the trajectory conditions. Figure 18 shows the B/I damping factor reduced from the dynamic wind tunnel tests using Equation 9. The B/I factor should be dependent on the transducer temperature and the head angular velocity, according to the laboratory tests the results of which are plotted in Figure 15. The transducer temperature was measured (at a point on the pitch potentiometer cover) with a thermocouple, during all wind tunnel tests. Table 2

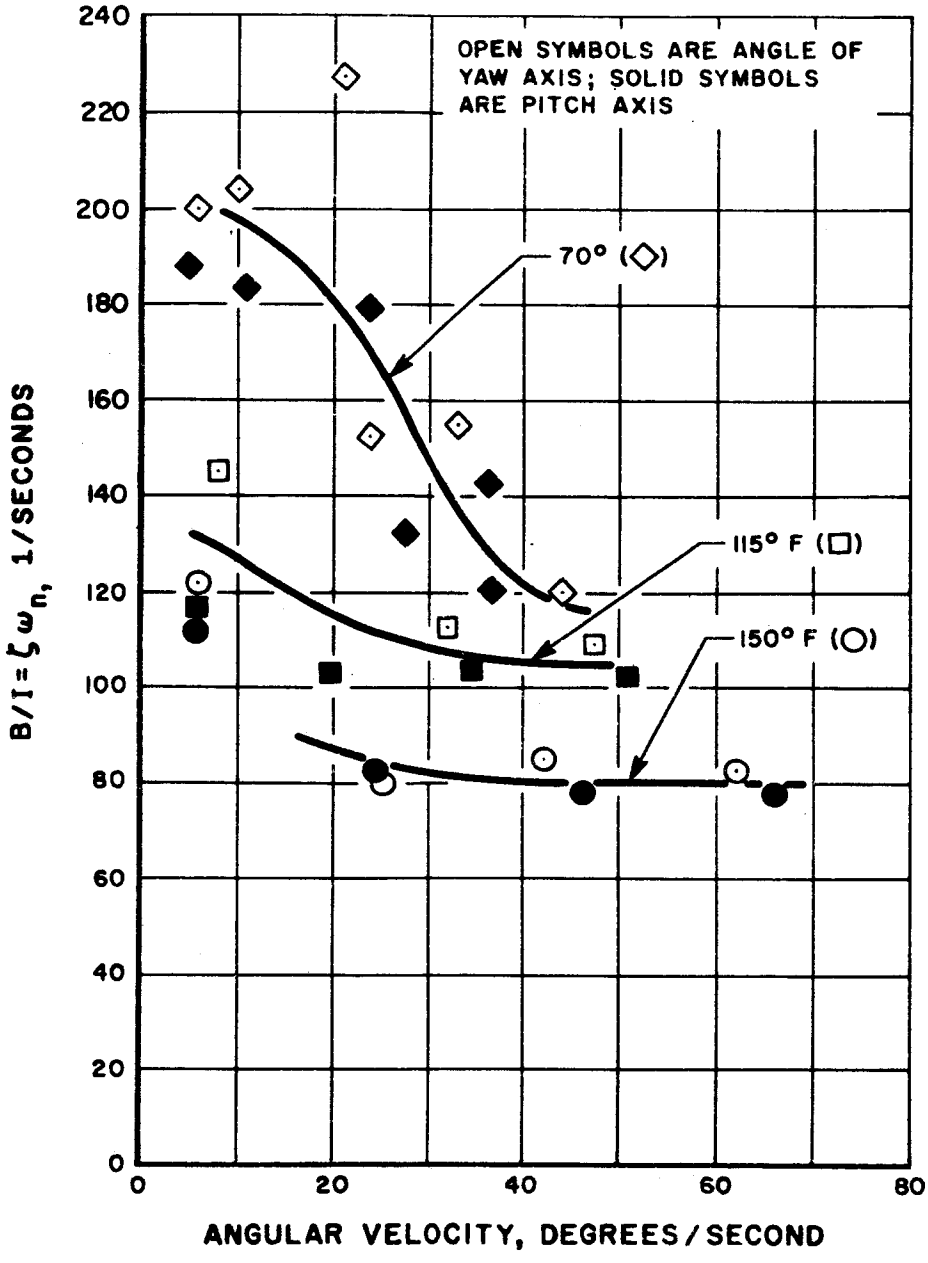

FIGURE 15 LABORATORY MEASUREMENTS OF VISCOUS DAMPING FACTOR OF TRANSDUCER S/N 119

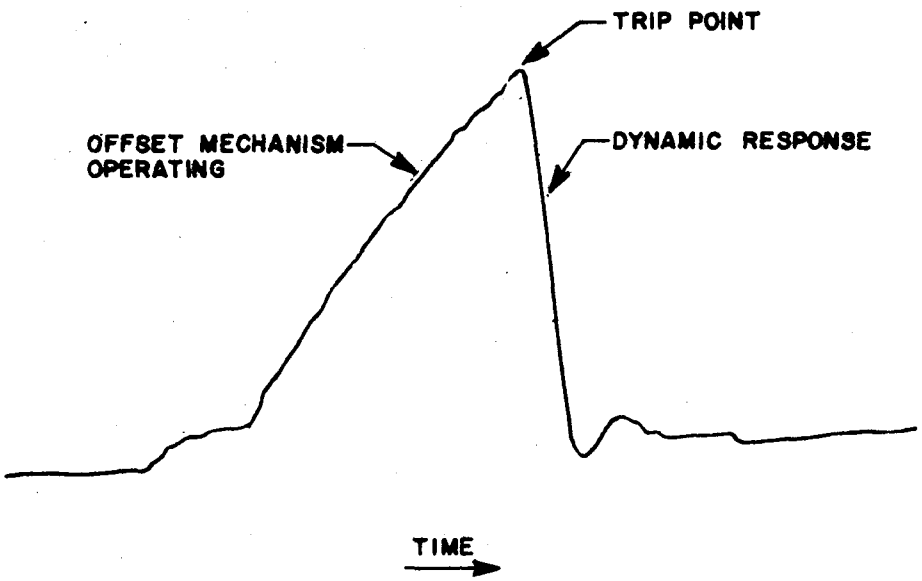

FIGURE 16 TYPICAL DYNAMIC RESPONSE OSCILLOGRAPH TRACE

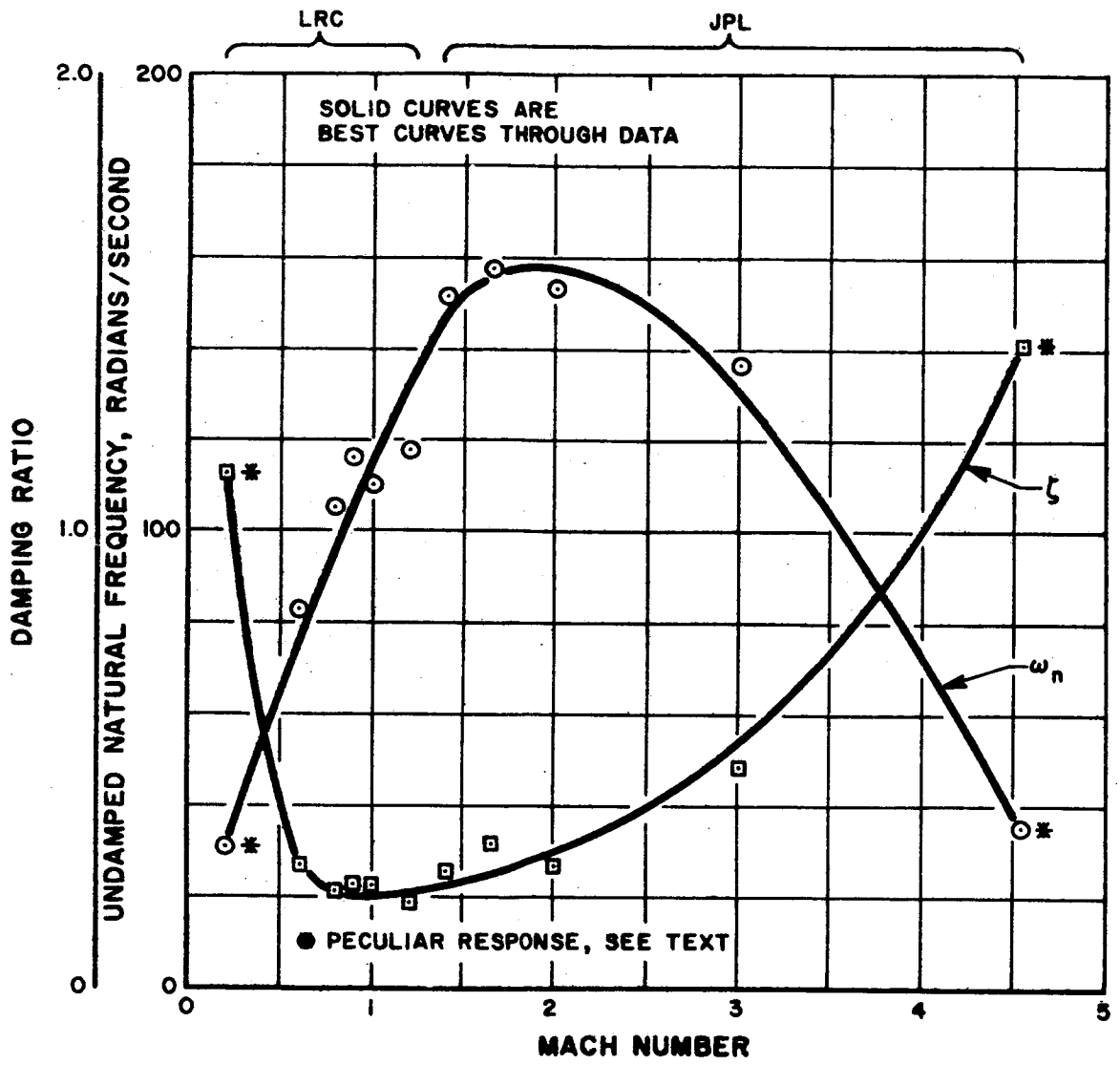

FIGURE 17 UNDAMPED NATURAL FREQUENCIES AND DAMPING RATIOS REDUCED FROM WIND TUNNEL DYNAMIC TEST

presents, for each Mach number condition, the average head angular velocity, the average of the transducer temperatures measured during the dynamic tests, and a B/I damping factor prediction based on Figure 15. (Because some of the angular velocities listed are greater than the range covered in Figure 15, the B/I factor is assumed to be constant with respect to velocity at velocities greater than 50 degrees per second.)

Temperatures in the LRC tunnel, on the whole, were higher than in the JPL tunnel; therefore, the predicted LRC damping factors are less, thus confirming the measured behavior shown in Figure 18. A point-by-point comparison is included in Figure 19. A substantial difference exists between the predicted B/I damping factor and the measured factor in the vicinity of Mach 1.

In the following a comparison is made between the magnitude of the B/I damping factor difference and the magnitude of the heat rate into the viscous damping fluid as a result of random motion of the transducer head. The data are not sufficient at this time to prove that this is the cause of the low B/I factor.

Turbulence (as discussed in Section III B) was also greatest in the vicinity of Mach 1. As a result of the energy dissipation effect of the viscous dampers, turbulence during the wind tunnel tests will transfer heat to the damping fluid. The rate of this heat transfer can be accurately determined from the oscillograph records, which show angle of pitch variation due to turbulence. At each wind tunnel condition, the heat rate was measured by fitting the best sine wave to the turbulence shown on the oscillograph trace. If the response is a pure sine wave, the heat rate is proportional to $(\theta_0\omega)^2$, where θ_0 and ω are the amplitude and the natural frequency of the fitted sine wave, respectively.* Assuming that the difference between the fluid temperature and measured transducer temperature (at one potentiometer cover) is exactly proportional to the heat rate, and assuming also that the fluid viscosity difference is proportional to the temperature difference, it is possible to interpret the measured heat rate in terms of a correction to the B/I damping factor -- that is, the B/I damping factor could be diminished, because of the damping fluid heating caused by airstream turbulence, by an amount proportional to the heat rate. The proportionality constant that provides the best correction is 418 seconds. If the $(\theta_0\omega)^2$ characteristics of the sine wave that fits the turbulence is multiplied by 418 seconds, a B/I correction results that best accounts for the difference between the predicted and measured B/I factors. For comparison, this correction for turbulence is shown with the difference between the predicted and measured B/I factor in Figure 19. Additional investigations of the phenomena energy dissipation through internal heating are being conducted at this time.

Transducer temperature, effective head angular velocity, and possibly turbulence level must all be considered in using the results of the foregoing to predict an in-flight damping factor in Transducer P/N 108760-E. It is

*θ_0 is measured in radians and ω is measured in radians per second.

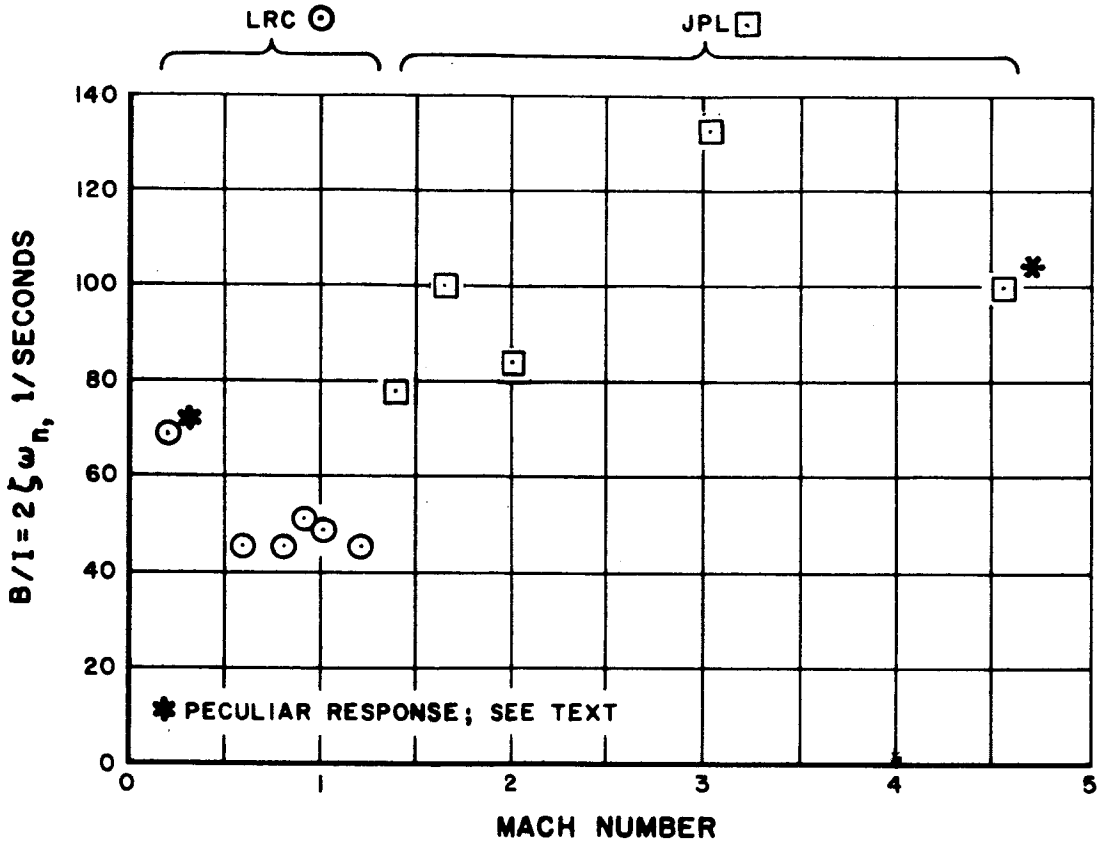

FIGURE 18 DAMPING FACTOR MEASURED IN WIND TUNNEL

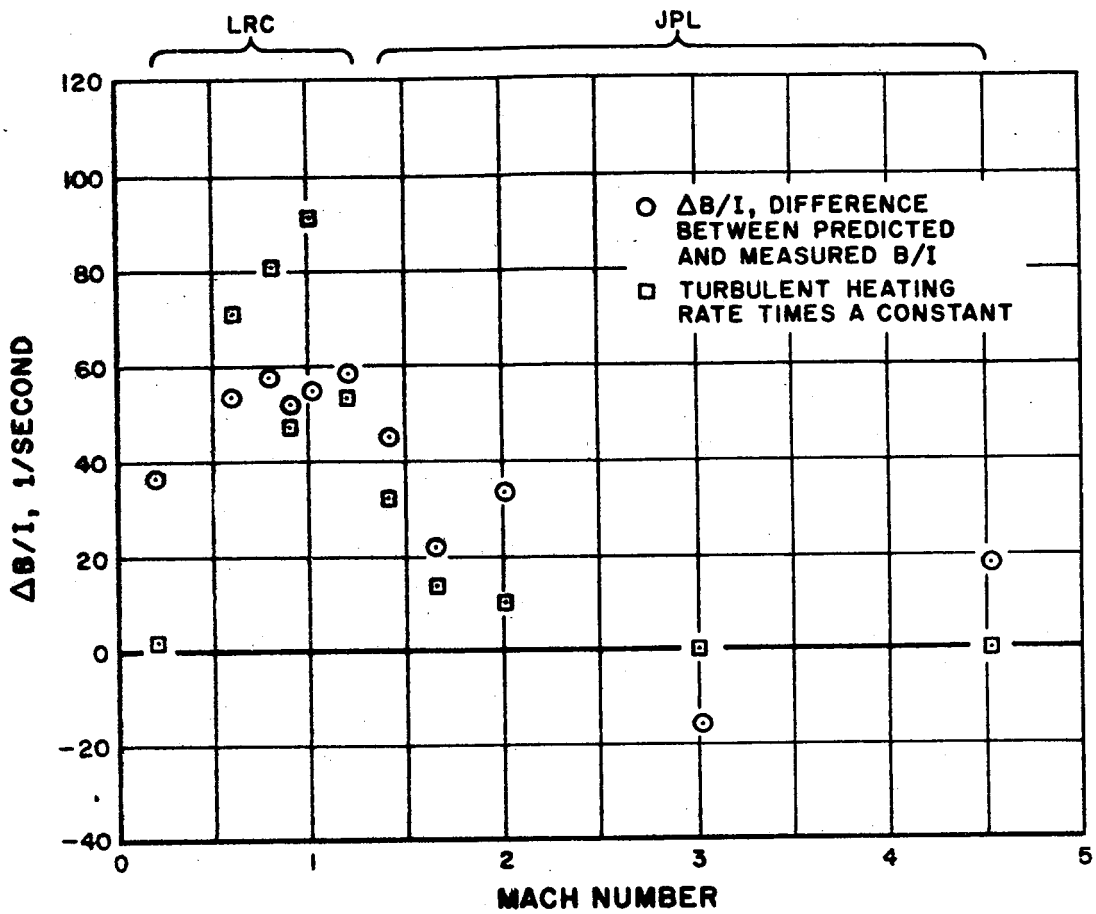

FIGURE 19 DIFFERENCE BETWEEN PREDICTED AND MEASURED DAMPING FACTORS, AND CORRECTIONS PROPORTIONAL TO TURBULENT HEATING RATE

TABLE 2 DAMPING FACTOR PREDICTIONS FROM LABORATORY MEASUREMENTS

Location of Tests	Mach Number	Head Velocity (degrees/sec)	Transducer Temperature (° F)	B/I (1/sec)
LRC	0.2	29.7	116	107
	0.6	79.5	117	100
	0.8	101	111	104
	0.9	112	111	104
	1.0	106	110	105
	1.2	113	110	105
JPL	1.40	146	76	125
	1.65	151	80	122
	2.01	148	87	118
	3.01	131	86	117
	4.54	33.6	91	117

expected, however, that the turbulence level in flight will not be as great as that experienced in the wind tunnel. It may be that the temperature and head velocity correlations alone (using Figure 15) will suffice. In the following a relationship is derived which allows comparison of the measured undamped natural frequency with that corresponding to the previously established torque coefficient shown in Figure 13.

As previously indicated, the aerodynamic spring constant, K, is equal to $dT/d\theta$ (Equation 1). Combining the relationships of Equations 1 and 7, it can be shown that the ratio of the undamped natural frequency and the square root of dynamic pressure is a unique function of C_{M_θ}, as follows:

$$\frac{\omega_n}{\sqrt{q}} = \sqrt{C_{M_\theta}} \sqrt{\frac{A^{3/2}}{I}} \tag{10}$$

Using Equation 10, the undamped natural frequency data determined from the dynamic tests are all combined with the measured dynamic pressure at each tunnel condition (plotted in Figure 5). Figure 20 shows the natural frequency data interpreted in this way. The solid curve is the square root of the torque coefficient derivative plotted in Figure 13 (determined from MSFC-supplied curves).

At the tunnel conditions corresponding to Mach 0.2 and Mach 4.54, an over-damped response was observed. The response at these two conditions did not follow what would be expected of a pure second-order system. Figure 21 shows one of the Mach 0.2 oscillograph traces, with the pure second-order response that was fitted to the first part of the curve. It is to be noted that a marked decrease in the slope occurs about halfway down. This inexplicable phenomenon occurred in all data from all 11 tests at Mach 0.2 and 4.54, in which both transducers and both axes of each were used. All the natural frequency and damping ratio data from tests at Mach 0.2 and 4.54 were interpreted, using only the first parts of the curves.

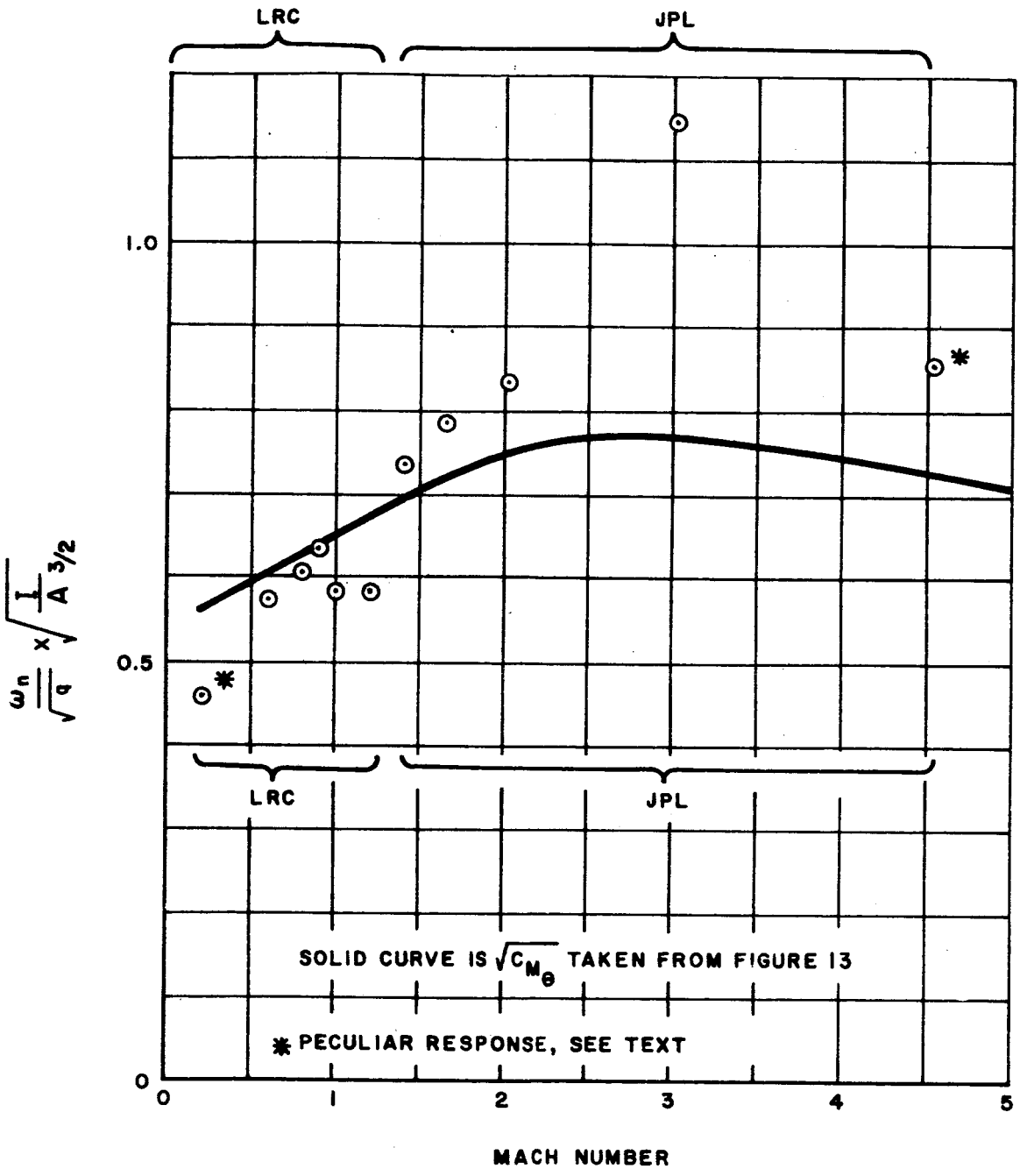

FIGURE 20 RATIO OF UNDAMPED NATURAL FREQUENCY AND THE SQUARE ROOT OF DYNAMIC PRESSURE

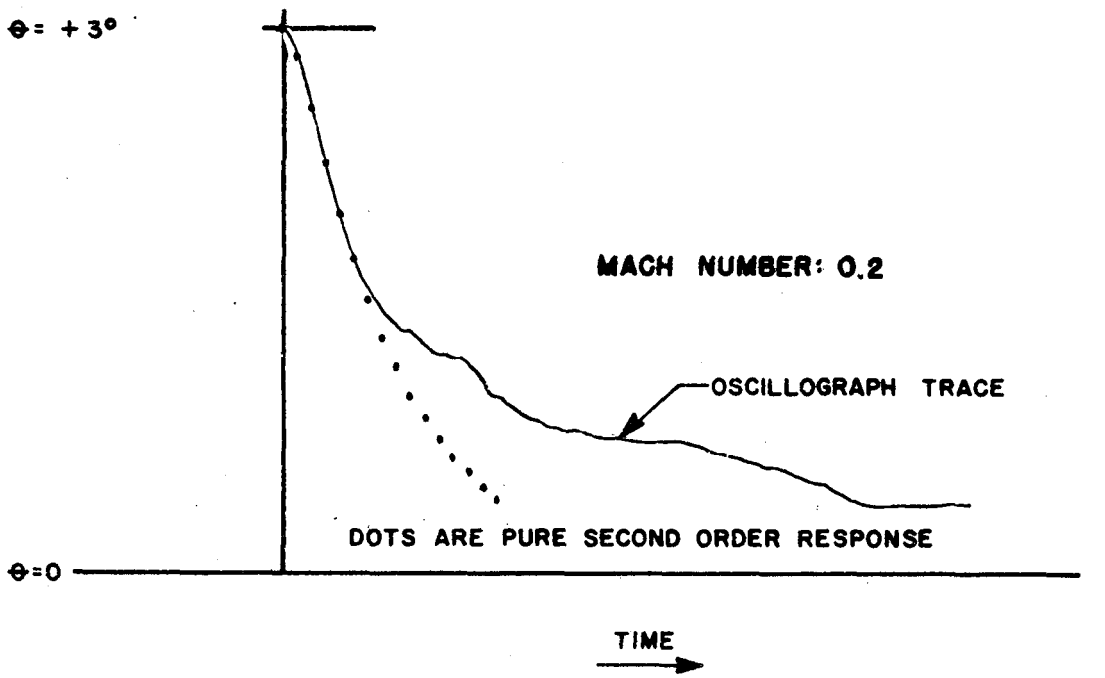

FIGURE 21 DYNAMIC RESPONSE TYPICAL OF ALL DATA OF TESTS AT MACH 0.2 AND 4.54

SECTION V. CONCLUDING REMARKS

The Edcliff 4-15 Angle of Pitch and Yaw Transducer has been wind tunnel tested over the Mach number and corresponding total pressure range of a typical liquid-fueled booster. Static and dynamic parameters have been determined which can be used for future prediction of the in-flight characteristics of the transducer.

The aerodynamic-to-mechanical misalignment was determined for one sensor to be 0.05 degree. Variation in the mechanical-to-electrical alignment was as great as 0.18 degree. It is appropriate to assume that the two misalignments are randomly distributed from transducer to transducer; therefore the root-sum-square of 0.05 and 0.18 degree is a measure of the total probable aerodynamic-to-electrical misalignment. The root-sum-square is 0.19 degree.

At Mach numbers greater than 1.40, the output-input relationship is linear within 0.4 degree; in the transonic region it is linear within 0.9 degree. If greater accuracy is required the calibration relationships given in Table 1 can be used.

The natural frequency varied from 32 to 157 radians per second for the tested Mach number and pressure conditions. The natural frequency history can be predicted for future trajectories from the Mach number and pressure histories of the trajectory.

The damping ratio varied from 0.2 to 1.4 critical. The damping ratio can be predicted for future flights from the Mach number and pressure histories and laboratory measurements of the B/I damping factor of the particular transducer.

SECTION VI. REFERENCES

1. "Characteristics of Nine Research Wind Tunnels of Langley Aeronautical Laboratory," 1957, NASA Washington Hdqtrs., file N 55488.

2. "Wind Tunnel Facilities at the Jet Propulsion Laboratory," JPL Release No. 34-247, California Institute of Technology, April 1961.

3. Minzner, R. A.; Champion, K. S. W.; and Pond, H. L.; "The 1959 ARDC Model Atmosphere."

4. "Equations, Tables, and Charts for Compressible Flow," NACA Report 1135, Ames Research Staff, Ames Aeronautical Laboratory, Moffett Field, California, 1953.

5. M. A. Silveira, et al, "Results of an Experimental Investigation of Small Viscous Dampers," NACA Technical Note 4257, June 1958.

APPROVAL MTP-AERO-63-34

WIND TUNNEL AND LABORATORY TESTS ON THE EDCLIFF 4-15
ANGLE OF PITCH AND YAW TRANSDUCER SUMMARY REPORT

AEROBALLISTICS DIVISION

The information in this report has been reviewed for security classification. Review of any information concerning Department of Defense or Atomic Energy Commission programs has been made by the MSFC Security Classification Officer. This report, in its entirety, has been determined to be unclassified.

OSCAR C. HOLDERER
Chief, Experimental Aerodynamics Branch

E. D. GEISSLER
Director, Aeroballistics Division

DISTRIBUTION MTP-AERO-63-34

M-DIR

M-DEP-DIR

M-SAT
Mr. Fikes

M-ASTR-N
Mr. Moore

M-AERO-DIR
Dr. Geissler

M-AERO
Mr. Reed, -TS
Mr. Murphree,-TS
Mr. Dahm, -A
Dr. Speer, -F
Mr. Holderer, -E
Mr. May, -E
Mr. Ballance, -E
Mr. Baur, -E (8)

M-MS-IP

M-MS-IPL (8)

M-MS-H

M-HME-P

M-PAT

EXTERNAL

Nortronics
Research Park
Palos Verdes Estates, California

Commander
Arnold Engineering Development Center
Arnold Air Force Station, Tennessee

EXTERNAL (Cont'd)

Jet Propulsion Laboratory
California Institute of Technology
4800 Oak Grove Drive
Pasadena, California

National Aeronautics and Space Administration
Ames Research Center
Moffett Field, California

National Aeronautics and Space Administration
Flight Research Center
P. O. Box 273
Edwards, California

National Aeronautics and Space Administration
Goddard Space Flight Center
Greenbelt, Maryland

National Aeronautics and Space Administration
Langley Research Center
Langley Field, Virginia
Attn: Mr. Henry Reichle, Jr.

Scientific and Technical Information Facility (2)
ATTN: NASA Representative (S-AK/RKT)
P. O. Box 5700
Bethesda, Maryland